A Separation Method for Multicomponent Nonstationary Signals with Crossover Instantaneous Frequencies*

Lin Li[1], Ningning Han[2], Qingtang Jiang[3], and Charles K. Chui[4]

Feb 8, 2020
(submitted to IEEE Trans IT on Feb 14, 2020, ms # IT-20-0113)

1. School of Electronic Engineering, Xidian University, Xi'an, China
2. Department of Mathematics, Hong Kong Baptist University, Hong Kong
3. Department of Math and CS, University of Missouri-St. Louis, St. Louis, USA
4. College of Mathematics and Statistics, Shenzhen University, China
and Department of Mathematics, Hong Kong Baptist University, Hong Kong

Abstract

In nature and engineering world, the acquired signals are usually affected by multiple complicated factors and appear as multicomponent nonstationary modes. In such and many other situations, it is necessary to separate these signals into a finite number of monocomponents to represent the intrinsic modes and underlying dynamics implicated in the source signals. In this paper, we consider the separation of a multicomponent signal which has crossing instantaneous frequencies (IFs), meaning that some of the components of the signal overlap in the time-frequency domain. We use a kernel function-based complex quadratic phase function to represent a multicomponent signal in the three-dimensional space of time, frequency and chirp rate, to be called the localized quadratic-phase Fourier transform (LQFT). We analyze the error bounds for IF estimation and component recovery with LQFT. In addition, we propose a matched-filter along certain specific time-frequency lines with respect to the chirp rate to make nonstationary signals be further separated and more concentrated in the three-dimensional space of LQFT. Based on the approximation of source signals with linear frequency modulation modes at any local time, we introduce an innovative signal reconstruction algorithm which is suitable for signals with crossing IFs. Moreover, this algorithm decreases component recovery errors when the IFs curves of different components are not crossover, but fast-varying and close to one and other. Numerical experiments on synthetic and real signals show our method is more accurate and consistent in signal separation than the empirical mode decomposition, synchrosqueezing transform, and other approaches.

*This work is partially supported by the Hong Kong Research Council, under Projects ♯ 12300917 and ♯ 12303218, and HKBU Grants ♯ RC-ICRS/16-17/03 and ♯ RC-FNRA-IG/18-19/SCI/01, and by the Simons Foundation, under grant ♯ 353185.

Keywords: *Time frequency analysis, localized quadratic-phase Fourier transform, separation of multicomponent signals with crossing instantaneous frequencies.*

1 Introduction

This paper studies blind source nonstationary signal separation in which a nonstationary signal is represented as a superposition of Fourier-like oscillatory modes:

$$x(t) = A_0(t) + \sum_{k=1}^{K} x_k(t), \quad x_k(t) = A_k(t)\cos\big(2\pi\phi_k(t)\big), \tag{1}$$

with $A_k(t), \phi_k'(t) > 0$ and $A_k(t)$, $\phi_k'(t)$ varying more slowly than $\phi_k(t)$. Such a representation, called an adaptive harmonic model (AHM) representation, is important for extracting information, such as the underlying dynamics, hidden in the nonstationary signal, with the trend $A_0(t)$, instantaneous amplitudes (IAs) $A_k(t)$ and the instantaneous frequencies (IFs) $\phi_k'(t)$ being used to describe the underlying dynamics.

In nature, many real-world phenomena that can be formulated as signals (or in terms of time series) are often affected by a number of factors and appear as time-overlapping multicomponent signals in the form of (1). A natural approach to understand and process such phenomena is to decompose, or even better, to separate the multicomponent signals into their basic building blocks $x_k(t)$ (called components or sub-signals) for extracting the necessary features. Also, for radar, communications, and other applications, signals often appear in multicomponent modes. Since these signals are mainly nonstationary, meaning the amplitudes and/or phases of some or all components change with the time, there have been few effective rigorous methods available for decomposition of them.

The empirical mode decomposition (EMD) algorithm along with the Hilbert spectrum analysis (HSA) is a popular method to decompose and analyze nonstationary signals [1]. EMD works like a filter bank [2, 3] to decompose a nonstationary signal into a superposition of intrinsic mode functions (IMFs) and a trend, and then the IF of each IMF is calculated by HSA. There are many articles studying the properties of EMD and variants of EMD have been proposed to improve the performance, see e.g. [2]-[13]. In particular, the separation ability of EMD was discussed in [4], which shows that EMD cannot decompose two components when their frequencies are close to each other. The ensemble EMD (EEMD) was proposed to suppress noise interferences [5]. The original EMD was extended to multivariate signals in [6, 7, 3]. Alternative sifting algorithms and formulations for EMD were introduced in [8] and [10]. Similar to the EMD filter bank, the wavelet filter bank for signal decomposition was proposed in [11], called empirical wavelet transform. An EMD-like sifting process was recently proposed in [12] to extract signal components in the linear

time-frequency (TF) plane one by one. EMD is an efficient data-driven approach and no basis of functions is required. A weakness of EMD or EEMD is that it can easily lead to mode mixtures or artifacts, namely undesirable or false components [14]. In addition, there is no mathematical theorem to guarantee the recovery of the components.

Time-frequency analysis is another method to separate multicomponent signals, which is widely used in engineering fields such as communication, radar and sonar as a powerful tool for analyzing signals [15]. Time-frequency signal analysis and synthesis using the eigenvalue decomposition method have been studied [16, 17, 18]. Recently the synchrosqueezing transform (SST) was developed in [19] to provide mathematical theorems to guarantee the component recovery of nonstationary multicomponent signals. The SST, which was first introduced in 1996, intended for speech signal separation [20], is based on the continuous wavelet transform (CWT). The short-time Fourier transform (STFT)-based SST was also proposed in [23] and further studied in [24, 25]. SST provides an alternative to the EMD method and its variants, and it overcomes some limitations of the EMD and EEMD schemes [26, 27]. SST has been used in machine fault diagnosis [28, 29], crystal image analysis [30, 31], welding crack acoustic emission signal analysis [32], and medical data analysis [33, 34, 35].

SST works well for sinusoidal signals, but not for broadband time-varying frequency signals. To provide sharp representations for signals with significantly frequency changes, two methods were proposed. One is the matching demodulation transform-based SST (or called the instantaneous frequency-embedded SST) proposed in [36, 37] which changes broadband signals to narrow-band signals (see also [38]). The instantaneous frequency-embedded SST proposed in [37] preserves the IFs of the original signals. The other method is the 2nd-order SST introduced in [39] and [40]. The higher-order FSST was presented in [41] and [42], which aims to handle signals containing more general types. Very recently an adaptive SST with a time-varying parameter were introduced in [43, 44]. They obtained the well-separated condition for multicomponent signals using the linear frequency modulation to approximate a nonstationary signal at any local time. In addition, theoretical analysis of adaptive SST was obtained in [45]. SST with a time-varying window width has also been studied in [46, 47].

To recover individual component $x_k(t)$, the SST method consists of two steps. First IF $\phi_k'(t)$ of $x_k(t)$ is estimated from the SST plane. Secondly, $x_k(t)$ is computed by a definite integral along each estimated IF curve on the SST plane. The reconstruction accuracy for $x_k(t)$ depends heavily on the accuracy of the IFs estimation carried out in the first step. On the other hand, a direct time-frequency approach, called signal separation operator (SSO), was introduced in [48] for multicomponent signal separation. In SSO approach, the components are reconstructed simply by substituting the time-frequency ridge to SSO.

While SST and SSO are mathematically rigorous on IF estimation and component recovery,

both of them require that the components $x_k(t)$ are well-separated in the time-frequency plane, namely IFs of $x_k(t)$ satisfy

$$\phi_k'(t) - \phi_{k-1}'(t) \geq 2\triangle,\ 2 \leq k \leq K, \tag{2}$$

for some $\triangle > 0$. In many applications, multicomponent signals are overlapping in the time-frequency plane, that is the IFs of its components are crossover. For example, in radar signal processing, the micro-Doppler effects are represented by highly nonstationary signals, when the target or any structure on the target undergoes micro-motion dynamics, such as mechanical vibrations, rotations, or tumbling and coning motions [49, 50]. Fig.1 shows simulated micro-Doppler modulations (two sinusoidal signals) induced by two target's tumbling motions and their short-time Fourier transforms (SFTFs). In practice we need to recover each components or at least the main body signature corresponding to the target's motion in the radar signal processing.

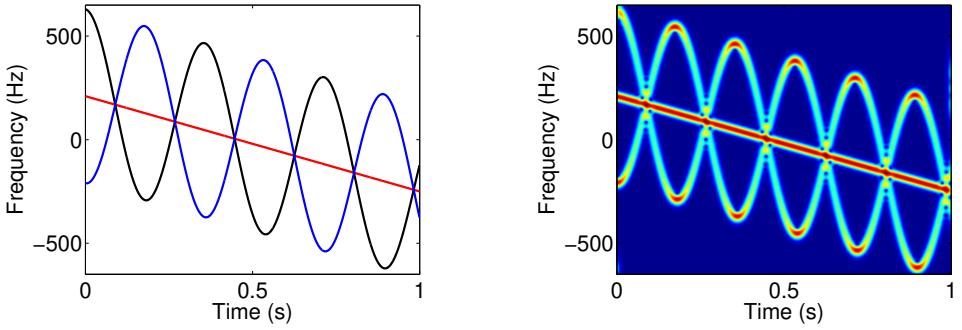

Figure 1: Micro-Doppler modulations induced by target's tumbling (Right) and their STFTs (Left).

We say two components $x_{k-1}(t)$ and $x_k(t)$ in (1) are overlapping in time-frequency plane when $t = t_0$ or the IF curves of them are crossing at $t = t_0$ if

$$\phi_{k-1}'(t_0) = \phi_k'(t_0) \text{ and } \phi_{k-1}''(t) \neq \phi_k''(t) \text{ for } t \in [t_0 - \delta_1, t_0 + \delta_1],$$

where δ_1 is a positive number. In this paper we consider multicomponent signals of the form (1) satisfying

$$|\phi_k'(t) - \phi_\ell'(t)| + \rho|\phi_k''(t) - \phi_\ell''(t)| \geq 2\triangle, \tag{3}$$

where $\rho \geq 0$ is a number decided by the user and $\triangle > 0$ is called the separation resolution. When $\rho = 0$, (3) is reduced to the well-separated condition (2) required for SST and SSO. Condition (3) allows the IFs of some components $x_k(t)$ to cross as long as their chirp rates $\phi_k''(t)$ are different near the time t_0 where IFs crossing occurs.

To separate signals overlapping in the time-frequency plane, we propose in this paper a kernel-based method, called the localized quadratic-phase Fourier transform (LQFT). LQFT is a generalization of the adaptive STFT from two-dimensional setting to the three-dimensional space of

time, frequency and chirp rate. We will present a matched-filter along the specific time-frequency lines associated with the chirp rate to make IFs crossover components be further separated and more concentrated in the three-dimensional space of LQFT. In addition, based on the approximation of source signals with linear-frequency-modulation modes at any local time, we propose an innovative signal reconstruction algorithm which is more suitable for signals with crossing IFs. Moreover, when the IFs curves of different components are not crossover, but fast-varying and close to each other, our reconstruction algorithm will decrease the recovery errors significantly.

Some methods have been proposed to estimate the IFs of nonstationary signals with crossover IFs. For example, the time-frequency distribution (with a cross-term) [51] was used to estimate IFs. [52] introduced an intrinsic chirp component decomposition to recover the instantaneous amplitude, and proposed a method called the ridge path regrouping to estimate IFs. [50] developed a compressive sensing approach to recover stationary narrowband signals contaminated by strong nonstationary signals. The LQFT defined in Section 3 uses a kind of parametric time-frequency analysis, see the local polynomial Fourier in [53, 54, 55]. The kernel for LQFT seems like a kind of chirplet transform introduced in [56] (also see some variants in [57]-[59]). However, our algorithm addresses the inverse transform and aims to decompose multicomponent signals with fasting-varying, even crossing IFs, which is different from the existing chirplet transforms. Most importantly, we provide a mathematically rigorous theorem which guarantees the recovery of components for multicomponent signal satisfying (3) with the LQFT approach. To our best knowledge, there is no other paper in the literature has established mathematical theorems to guarantee the recovery of the components overlapping in the time-frequency plane. Furthermore, we use a matched-filter along the specific time-frequency lines respect to the chirp rate to make different components be further separated and more concentrated in the three dimensional space of LQFT.

The remainder of this paper is organized as follows. In Section 2, we first review the signal separation methods by SST and SSO. After that we state the problem of recovering sub-signals with crossing IFs. In Section 3, we introduce LQFT and filtered LQFT for separating multicomponent signals with fast-varying and crossing IFs. We present the numerical experiments and analysis in Section 4. A conclusion is then presented in Section 5.

2 Problem statement

The (modified) STFT of signal $x(t) \in L_2(\mathbb{R})$ with a window function $g(t) \in L_2(\mathbb{R})$ is defined by,

$$V_x(t,\eta) := \int_{\mathbb{R}} x(\tau) g(\tau - t) e^{-i2\pi\eta(\tau - t)} d\tau, \tag{4}$$

If $g(0) \neq 0$, then the original signal $x(t)$ can be recovered back from its STFT:

$$x(t) = \frac{1}{g(0)} \int_{\mathbb{R}} V_x(t,\eta) d\tau. \tag{5}$$

For multicomponent signal $x(t)$ in (1) satisfying the separation condition (2), the sub-signal $x_k(t)$ can be recovered by

$$x_k(t) \approx \frac{1}{g(0)} \int_{|\eta - \phi_k'(t)| < \Gamma_1} V_x(t,\eta) d\eta, \tag{6}$$

for some $\Gamma_1 > 0$.

To enhance the time-frequency resolution and concentration, the idea of SST is to reassign the frequency variable. As in [23], denote

$$\omega_x(t,\eta) := \frac{\frac{\partial}{\partial t} V_x(t,\eta)}{i2\pi V_x(t,\eta)}. \tag{7}$$

The quantity $\omega_x(t,\eta)$ is called the "phase transformation" [19]. The STFT-based SST is to reassign the frequency variable η by transforming STFT $V_x(t,\eta)$ of $x(t)$ to a quantity, denoted by $R_x(t,\eta)$, on the time-frequency plane:

$$R_x(t,\eta) := \int_{\{\xi : V_x(t,\xi) \neq 0\}} V_x(t,\xi) \delta\left(\omega_x(t,\xi) - \eta\right) d\xi. \tag{8}$$

One also has a reconstruction formula of $x_k(t)$ similar to (6) with $V_x(t,\xi)$ replaced by $R_x(t,\xi)$. Moreover, the second-order [39] and high-order [41] SSTs were introduced based on higher order phase transformations.

Observe that signal reconstructions with STFT and SST depend on the IF estimation of $\phi_k'(t)$ and a given threshold Γ_1, hence it is indirect. In contrast, signal separation operator (SSO) [48] extracts signal components via local frequencies directly. The SSO $T_{a,\delta}$, which is applied to signals x in (1), is defined by

$$\left(T_{a,\delta} x\right)(t,\theta) := \frac{1}{\hbar_a} \sum_{n \in \mathbb{Z}} x(t - n\delta) h\left(\frac{n}{a}\right) e^{i2\pi n\theta}, \tag{9}$$

where h is an admissible window function, $\theta \in [0,1]$ and $\delta, a > 0$ are parameters, with a so chosen that

$$\hbar_a := \sum_{n \in \mathbb{Z}} h\left(\frac{n}{a}\right) > 0. \tag{10}$$

For a multicomponent signal $x(t)$ defined in (1), satisfying the well-separation condition (2), the set $\{\theta \in [0,1] : |\left(T_{a,\delta} x\right)(t,\theta)| > \Gamma_2\}$ can be expressed as a disjoint union of exactly K non-empty sets $\Theta_l, l = 1, 2, ..., K$, corresponding to the K components of $x(t)$. The sub-signal $x_k(t)$ can be reconstructed by,

$$\widehat{x}_k(t) = 2\Re e\left\{\left(T_{a,\delta} x\right)(t, \widehat{\theta}_k)\right\}, \tag{11}$$

where

$$\widehat{\theta}_k(t) = \arg\max_{\theta\in\Theta_k} |\left(T_{a,\delta}x\right)(t,\theta)|. \tag{12}$$

As mentioned in Section 1, to recover components $x_k(t)$ with SST or SSO, it is required all IFs of different components be separated from each other, namely they be far away from each other and non-crossing as shown in (2). There are few methods available can recover the components in (1) when the IFs are crossing. In particular, there is no theoretical theorem to guarantee the recovery of the waveforms of components when their IFs are crossover with only one observation $x(t)$ available. This paper is to provide a method to recover such nonstationary multicomponent signals and present theoretical analysis on the recovery error. Next let us consider an example to show the performances of EMD, SST, SSO and our method LQFT in separating a signal with crossover IFs.

Let $f(t)$ be the two-component signal introduced in [19]:

$$f(t) = f_1(t) + f_2(t) = \cos\left(t^2 + t + \cos(t)\right) + \cos(8t). \tag{13}$$

Here we let the sampling rate $F_s = 20$Hz and we only analyze the truncation signal on $t \in [0, 256/F_s]$, with 256 discrete sampling points. The instantaneous frequencies of $f_1(t)$ and $f_2(t)$ are $\phi_1'(t) = (2t + 1 - \sin(t))/(2\pi)$ and $\phi_2'(t) = 4/\pi$, respectively.

Fig.2 shows some recovery results of $f_1(t)$ and $f_2(t)$. Observe that compared to the STFT and the STFT-based SST, the 2nd-order SST of $f(t)$ represents this two-component signal with crossing IF curves much sharper and clearer. However, the existing methods including EMD [1], SST [24], the 2nd-order SST [39] and SSO [48] are unable to recover the waveforms $f_1(t)$ and $f_2(t)$ accurately, see the recovered f_1 and f_2 by these methods in Fig.2. Our proposed LQFT with Algorithm 1 provided in §3.2 can recover the two components accurately as shown in the 4th panels (from the left) in row 3 and row 4 respectively in Fig.2. Note that EMD, SST, 2nd-order SST and SSO all result in big recovery errors for either f_1 or f_2 around $t_0 = 3.38$ where IFs crossing occurs, while our method produces very small errors near t_0. The boundary effect is unavoidable for all methods since we only use the truncation signal for $0 \le t \le 12.8$ and the boundary extension has not be considered in this example. In addition, in this example we simply use the same Gaussian window with constant variance $\sigma = 1.6$ for STFT, SST, the 2nd-order SST, SSO and LQFT.

3 Signal separation with localized quadratic-phase Fourier transform (LQFT)

In this section we introduce LQFT and provide the main theorem on component recovery with LQFT. In addition, we introduce filtered LQFT to make IFs crossover components further sepa-

rated and more concentrated in the three-dimensional space of LQFT. Furthermore, we propose an algorithm based on LQFT to improve the performance of LQFT in signal separation.

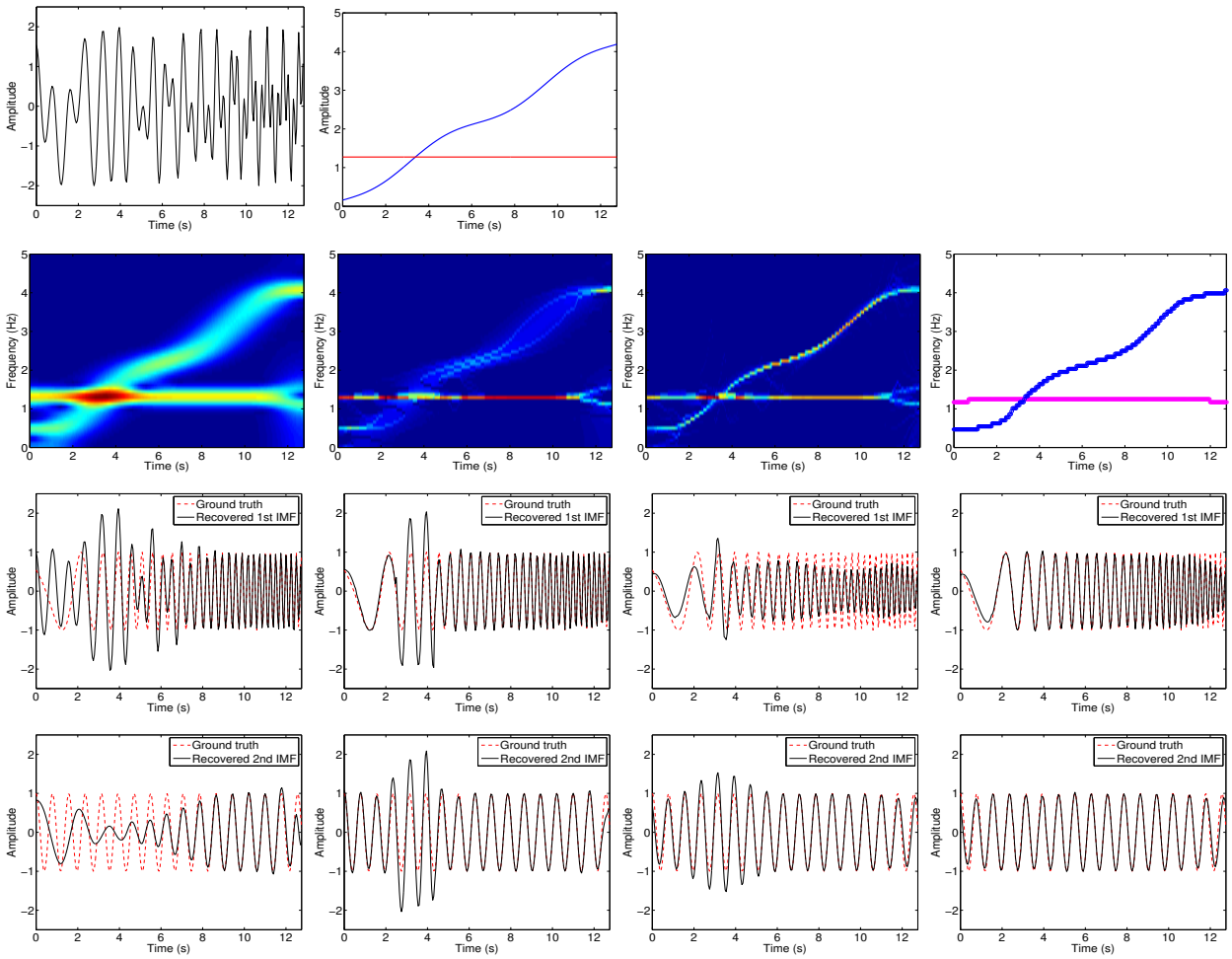

Figure 2: Results of component recovery of two-component signal $f(t)$ in (13). The source signal $f(t)$: Waveform and IFs (Top row, from left to right); Time-frequency diagrams: STFT, SST, 2nd-order SST and estimated IFs by LQFT (Second row, from left to right); Recovery results of $f_1(t)$ by different methods: EMD, 2nd-order SST, SSO and our proposed method (Third row, from left to right); Recovery results of $f_2(t)$ by different methods: EMD, 2nd-order SST, SSO and our proposed method (Bottom row, from left to right).

3.1 Main results

In this subsection, first we introduce LQFT. After that we define the class of IF crossover multicomponent signals which can be separated by LQFT and an admissible window function used in for signal separation. The main result, Theorem 1, will be followed then.

Definition 1. (LQFT) *The LQFT applied to a signal $x(t)$ is defined by*

$$\mathfrak{S}_x(t,\eta,\lambda) := \int_{\mathbb{R}} x(\tau)\mathcal{K}_\sigma(\tau-t,\eta,\lambda)d\tau = \int_{\mathbb{R}} x(t+\tau)\mathcal{K}_\sigma(\tau,\eta,\lambda)d\tau, \tag{14}$$

where

$$\mathcal{K}_\sigma(\tau,\eta,\lambda) := \frac{1}{\sigma}g\big(\frac{\tau}{\sigma}\big)e^{-i2\pi\eta\tau-i\pi\lambda\tau^2}, \tag{15}$$

and $g(t)$ is a window function and $\sigma>0$.

Observe that when $\lambda=0$, $\mathfrak{S}_x(t,\eta,\lambda)$ is the adaptive STFT considered in [43]. $\mathfrak{S}_x(t,\eta,\lambda)$ is also called a local polynomial Fourier transform, see [53, 54, 55]. Here we call it the localized quadratic-phase Fourier transform (LQFT). In addition, we can also regard $\mathfrak{S}_x(t,\eta,\lambda)$ as the continuous form of SSO (which is the adaptive STFT) after the quadratic term $e^{-i\pi\lambda\tau^2}$ is added to match the local change of a non-stationary signal. Thus we also call it the "matched" SSO.

LQFT represents a multicomponent signal in a three-dimension space of time, frequency and chirp rate. Note that when the IF curves of two components $x_{k-1}(t)$ and $x_k(t)$ are crossing, they may be well-separated in the three-dimensional space of LQFT since $\phi''_{k-1}(t)\neq\phi''_k(t)$ for t near the crossover time t_0. Thus a multicomponent signal with IFs crossover components could be well-separated and concentrated in the three-dimensional space of LQFT, and hence, it is feasible to propose to reconstruct its components by LQFT.

Definition 2. *For an $\alpha>0$, let $\mathcal{A}_\alpha$ denote the set consisting of (complex) adaptive harmonic models (AHMs) defined by*

$$x(t)=A_0(t)+\sum_{k=1}^{K}x_k(t)=\sum_{k=0}^{K}A_k(t)e^{i2\pi\phi_k(t)}, \tag{16}$$

with $A_k(t)\in L_\infty(\mathbb{R})$, $A_k(t)>0, \phi_k(t)\in C^3(\mathbb{R}), \inf_{t\in\mathbb{R}}\phi'_k(t)>0, \sup_{t\in\mathbb{R}}\phi'_k(t)<\infty$, and $A_k(t),\phi_k(t)$ satisfying

$$|A_k(t+\tau)-A_k(t)|\le\alpha^3B_1|\tau|A_k(t),\quad k=0,\cdots,K, \tag{17}$$

$$\sup_{t\in\mathbb{R}}|\phi'''_k(t)|\le\alpha^7B_2,\quad k=0,\cdots,K \tag{18}$$

where B_1,B_2 are some positive constants independent of α.

In Definition 2 and in the rest of this paper, we also write the trend $A_0(t)$ as $x_0(t) = A_0(t)e^{i2\pi\phi_0(t)}$ with $\phi_0(t) = 0$. In the real world, most signals are real-valued. Here for simplicity of presentation of the main result, Theorem 1, and its proof, we consider complex AHM given in the form of (16). The statement of Theorem 1 and its proof still hold for (real-valued) AHM given in (1) by extra agruments.

Denote

$$\mu = \mu(t) := \min_{0\le k\le K} |A_k(t)|, \quad M = M(t) := \sum_{k=0}^{K} |A_k(t)|. \tag{19}$$

For a window function $g \in L_1(\mathbb{R})$, denote

$$\breve{g}(\eta,\lambda) := \int_{\mathbb{R}} g(\tau) e^{-i2\pi\eta\tau - i\pi\lambda\tau^2} d\tau. \tag{20}$$

$\breve{g}(\eta,\lambda)$ is called a polynomial Fourier transform of g [55, 60].

Definition 3. (**Admissible window function**) *A function $g(t) \ge 0$ is called an admissible window function if $\int_{\mathbb{R}} g(t)dt = 1$, supp$(g) \subseteq [-N, N]$ for some $N > 0$, and satisfies the following conditions.*

(a) *There exists a constant C such that*

$$|\breve{g}(\eta,\lambda)| \le \frac{C}{\sqrt{|\eta| + |\lambda|}}, \ \forall \eta,\lambda \in \mathbb{R}. \tag{21}$$

(b) *If there exists a constant D such that*

$$1 - |\breve{g}(\eta,\lambda)| \le D\varepsilon, \tag{22}$$

holds for sufficiently small $\varepsilon > 0$ and (η,λ) in the neighborhood of $(0,0)$, then η and λ must satisfy

$$|\eta| = o(1) \ \text{ and } \ |\lambda| = o(1) \ \text{ as } \ \varepsilon \to 0. \tag{23}$$

When g is the Gaussian function given by

$$g(t) = \frac{1}{\sqrt{2\pi}}\, e^{-\frac{t^2}{2}}, \tag{24}$$

then (refer to [15, 43, 44])

$$\breve{g}(\eta,\lambda) = \frac{1}{\sqrt{1 + i2\pi\lambda}} e^{-\frac{2\pi^2\eta^2}{1+i2\pi\lambda}}. \tag{25}$$

One can verify that $|\breve{g}(\eta,\lambda)| = \frac{1}{(1+4\pi^2\lambda^2)^{1/4}} e^{-\frac{2\pi^2\eta^2}{1+(2\pi\lambda)^2}}$ satisfies conditions (a)(b) in Definition 3.

Observe that for an admissible window function g, we have

$$|\breve{g}(\eta,\lambda)| \le \breve{g}(0,0) = 1.$$

In addition, from (21), we have

$$|\breve{g}(\eta,\lambda)| \le \frac{L}{\sqrt{|\eta|+\rho|\lambda|}},\ \forall \eta,\lambda\in\mathbb{R}, \tag{26}$$

where $L=\max(1,\sqrt{\rho})C$, and $\rho\ge$ is the number in (3).

Theorem 1. *Let $x(t)\in\mathcal{A}_\alpha$ for some $\alpha>0$, and $\mathfrak{S}_x(t,\eta,\lambda)$ be the LQFT of $x(t)$ with an admissible window function g. Let $\sigma:=\frac{c_0}{\alpha^2}$ for some $c_0>0$. If $\phi_k'(t), 0\le k\le K$ satisfy (3) for some $\rho\ge 0$, $\triangle>0$ and*

$$\alpha \le \min\Big\{\frac{\mu}{4Mc_0N(B_1+\frac{\pi}{3}B_2c_0^2N^2)}, \frac{\mu\sqrt{c_0\triangle}}{4ML}\Big\}, \tag{27}$$

then the following statements hold.

(a) *The set $\mathcal{G}(t):=\{(\eta,\lambda):|\mathfrak{S}_x(t,\eta,\lambda)|\ge\mu/2\}$ can be expressed as a disjoint union of exactly $K+1$ non-empty sets*

$$\mathcal{G}_\ell(t):=\big\{(\eta,\lambda)\in\mathcal{G}(t):\sigma|\eta-\phi_\ell'(t)|+\rho\sigma^2|\lambda-\phi_\ell''(t)|\le\big(\frac{4LM}{\mu}\big)^2\big\},\ \ell=0,\cdots,K. \tag{28}$$

(b) *Let*

$$(\widehat{\eta}_\ell,\widehat{\lambda}_\ell):=\mathrm{argmax}_{(\eta,\lambda)\in\mathcal{G}_\ell(t)}|\mathfrak{S}_x(t,\eta,\lambda)|,\quad \ell=0,\cdots,K.$$

Then

$$\big||\mathfrak{S}_x(t,\widehat{\eta}_\ell,\widehat{\lambda}_\ell)|-A_\ell(t)\big|\le\alpha M\Big(\frac{L}{\sqrt{c_0\triangle}}+c_0NB_1+\frac{\pi}{3}B_2c_0^3N^3\Big), \tag{29}$$

$$|\widehat{\eta}_\ell-\phi_\ell'(t)|=\frac{1}{\sigma}o(1)=\alpha^2o(1),\quad |\widehat{\lambda}_\ell-\phi_\ell''(t)|=\frac{1}{\sigma^2}o(1)=\alpha^4o(1)\ \ \text{as}\ \alpha\to0^+, \tag{30}$$

$$\big|\mathfrak{S}_x(t,\widehat{\eta}_\ell,\widehat{\lambda}_\ell)-x_\ell(t)\big|\le o(1)+\alpha M\Big(\frac{L}{\sqrt{c_0\triangle}}+c_0NB_1+\frac{\pi}{3}B_2c_0^3N^3\Big), \tag{31}$$

as $\alpha\to0^+$.

The proof of Theorem 1 is provided in Appendix.

Remark 1. *The error bounds in (29) and (31) are related to*

$$M\big(\frac{L}{\sqrt{c_0\triangle}}+c_0NB_1+\frac{\pi}{3}B_2c_0^3N^3\big).$$

We shall choose c_0 such that the above quantity as small as possible. Considering that the third power c_0^3 of c_0 appears in this quantity, we shall choose $c_0\le1$. With $c_0\le1$, one may choose c_0 such that $\frac{L}{\sqrt{c_0\triangle}}=c_0NB_1$ with which $\frac{L}{\sqrt{c_0\triangle}}+c_0NB_1$ gains its minimum. Thus we may let

$$c_0=\min\Big(1,\big(\frac{L^2}{B_1^2N^2\triangle}\big)^{\frac{1}{3}}\Big).$$

□

Theorem 1 shows that we can use LQFT to separate a multicomponent signal, even when the IF curves of different components are crossover. More precisely, for a multicomponent signal $x \in \mathcal{A}_\alpha$, its sub-signal $x_\ell(t)$ can be reconstructed by

$$\widehat{x}_\ell(t) = \mathfrak{S}_x(t, \widehat{\eta}_\ell, \widehat{\lambda}_\ell),\ \ell = 1, 2, \cdots, K. \tag{32}$$

Especially for real-valued signals, we have

$$\widehat{x}_\ell(t) = \Re e\left\{\mathfrak{S}_x(t, \widehat{\eta}_\ell, \widehat{\lambda}_\ell)\right\},\ \ell = 1, 2, \cdots, K. \tag{33}$$

The trend in (16) can also be recovered by

$$\widehat{x}_0(t) = \mathfrak{S}_x(t, 0, 0) \tag{34}$$

for complex signals or

$$\widehat{x}_0(t) = \Re e\left\{\mathfrak{S}_x(t, 0, 0)\right\} \tag{35}$$

for real-valued signals.

Note that $\sigma = \frac{c_0}{\alpha^2}$. That is to get a smaller component recover error which is proportion to α, we need to increase the window length σ. However, for an arbitrary nonstationary signal, the recover error cannot be reduced just by relaying on increasing the parameter σ. To this regard, we propose a modified algorithm in the next subsection to reduce the recovery errors.

3.2 A modified algorithm derived from LFM approximation

From the uncertainty principle [15], one can get the minimum time-bandwidth product with a Gaussian window, which means the optimal two-dimensional resolution of time and frequency is attained when a Gaussian window is used. So next we consider the LQFT with the Gaussian window function given by (24).

When $x(t) \in \mathcal{A}_\alpha$, then Conditions (17) and (18) imply that each component $x_k(t)$ is well-approximated by linear frequency modulation (LFM) signals at any time t in the sense of (see Appendix)

$$x_k(t+\tau) \approx x_k(t) e^{i2\pi(\phi_k'(t)\tau + \frac{1}{2}\phi_k''(t)\tau^2)},\ t \in \mathbb{R}, \tag{36}$$

for $\tau \approx 0$. For a fixed t, the right side of (36), as a function of τ, is an LFM signal. Thus

$$\begin{aligned}
\mathfrak{S}_{x_k}(t, \eta, \lambda) &\approx \int_{\mathbb{R}} x_k(t) e^{i2\pi(\phi_k'(t)\tau + \frac{1}{2}\phi_k''(t)\tau^2)} \mathcal{K}_\sigma(\tau, \theta, \lambda) d\tau \\
&= x_k(t) \int_{\mathbb{R}} \frac{1}{\sigma} g\big(\frac{\tau}{\sigma}\big) e^{-i2\pi(\eta - \phi_k'(t))\tau - i\pi(\lambda - \phi_k''(t))\tau^2} d\tau \\
&= x_k(t)\, \breve{g}\left(\sigma(\eta - \phi_k'(t)), \sigma^2(\lambda - \phi_k''(t))\right) \\
&= \frac{1}{\sqrt{1 + i2\pi\sigma^2(\lambda - \phi_k''(t))}} x_k(t) e^{-\frac{2\pi^2\sigma^2}{1 + i2\pi\sigma^2(\lambda - \phi_k''(t))}(\eta - \phi_k'(t))^2} \text{ (by (25))} \\
&=: x_k(t) \mathbb{A}(\lambda - \phi_k''(t)) \Omega(\lambda - \phi_k''(t), \eta - \phi_k'(t)),
\end{aligned} \tag{37}$$

where $\mathbb{A}(\lambda) := \frac{1}{\sqrt{1+i2\pi\sigma^2\lambda}}$ and $\Omega(a,b) := e^{-\frac{2\pi^2\sigma^2}{1+i2\pi\sigma^2 a}b^2}$.

Thus by Theorem 1 and (32), if

$$\left(\widehat{\eta}_k, \widehat{\lambda}_k\right) = (\phi_k'(t), \phi_k''(t)),$$

we have,

$$\widehat{x}_k(t) = \mathfrak{S}_{x_k}(t, \widehat{\eta}_k, \widehat{\lambda}_k) \approx x_k(t). \tag{38}$$

Hence in this case sub-signals $x_k(t)$ can be separated and recovered from $\mathfrak{S}_{x_k}$ accurately. For a multicomponent signal $x(t)$, we need to find the extreme points $(\widehat{\eta}_\ell, \widehat{\lambda}_\ell), \ell = 1, 2, \cdots, K$ of $|\mathfrak{S}_{x_\ell}(t,\eta,\lambda)|$ with $(\eta,\lambda) \in \mathcal{G}_\ell$. Therefore, we first need to find these K non-empty sets $\mathcal{G}_\ell, \ell = 1, 2, \cdots, K$ as defined in Theorem 1 on the three-dimensional space $\mathfrak{S}_x(t,\eta,\lambda)$. However when the IF curves of two components $x_{\ell-1}(t)$ and $x_\ell(t)$ are crossing, $\mathcal{G}_{\ell-1}$ and $\mathcal{G}_\ell$ are not separated far to each other in the three-dimensional space of LQFT due to the fact that $|\mathfrak{S}_{x_k}(t,\eta,\lambda)|$ is not a fast-decay function with respect to the chirp rate λ. Next we use an example to explain this point.

Let $s(t)$ be a two-component signal given by

$$s(t) = s_1(t) + s_2(t) = \cos\left(2\pi c_1 t + \pi r_1 t^2\right) + \cos\left(2\pi c_2 t + \pi r_2 t^2\right). \tag{39}$$

Here we let sampling rate $F_s = 1$Hz and just deal with the truncation signal on $t \in [0, 255]$, with $N = 256$ discrete sampling points. Especially, we consider the case $c_1 = 15/N$, $c_2 = 43/N$, $r_1 = 43/N^2$ and $r_2 = -20/N^2$. Fig.3 shows the IFs and STFT of $s(t)$, and some special slices of the LQFT of the two-component signal $s(t)$ with the Gaussian window. Observe that when $\lambda = r_1$ or $\lambda = r_2$, $s_1(t)$ and $s_2(t)$ are well represented on the two time-frequency planes $|\mathfrak{S}_s(t,\eta,r_1)|$ and $|\mathfrak{S}_s(t,\eta,r_2)|$, respectively. In this example, we let $\sigma(t) = 0.1N$.

Now we focus on the crossing point of the two IFs of $s_1(t)$ and $s_2(t)$, which is located at around (t_0, η_0) with $t_0 = 114$ and $\eta_0 = 0.133$. From the 1st and 3rd panels in the bottom row of Fig.3, the two components appear to two separated peaks on the chirp rate-frequency and chirp rate-time planes, respectively, but not very clearly and sharply. Taking $t = t_0$ and $\eta = \eta_0$ in (37), we have

$$\begin{aligned}
\mathcal{L}(\lambda) &= |\mathfrak{S}_s(114, \eta_0, \lambda)| \\
&= \left| \frac{1}{2\sqrt{1 + i2\pi\sigma^2(\lambda - r_1)}} \tilde{s}_1(t) + \frac{1}{2\sqrt{1 + i2\pi\sigma^2(\lambda - r_2)}} \tilde{s}_2(t) \right| \\
&\approx \frac{1}{2\sqrt[4]{1 + 4\pi^2\sigma^4(\lambda - r_1)^2}} + \frac{1}{2\sqrt[4]{1 + 4\pi^2\sigma^4(\lambda - r_2)^2}},
\end{aligned}$$

where $\tilde{s}_k(t) = e^{i2\pi c_k t + i\pi r_k t^2}$ denotes the analytic signal of $s_k(t)$, $k = 1, 2$. Note that the two parts in $\mathcal{L}(\lambda)$ above are corresponding to $s_1(t)$ and $s_2(t)$, respectively, which are centered at

$\lambda = r_1 = 43/N^2$ and $\lambda = r_2 = -20/N^2$. Then let $t = 114$ and $\lambda = r_2$, we obtain

$$\mathcal{T}(\eta) = |\mathfrak{S}_s(114, \eta, r_2)| \approx \frac{1}{2} e^{-2\pi^2\sigma^2(\eta-\eta_0)^2}.$$

Compared to $\mathcal{T}(\eta)$, $\mathcal{L}(\lambda)$ is a slowly attenuated function from the two extrema located at $\lambda = r_1$ and $\lambda = r_2$. This explains why there are two components which not well separated in either the 1st or the 3rd panel in the bottom row of Fig.3, while there is only one component in the 4th panel of the top row.

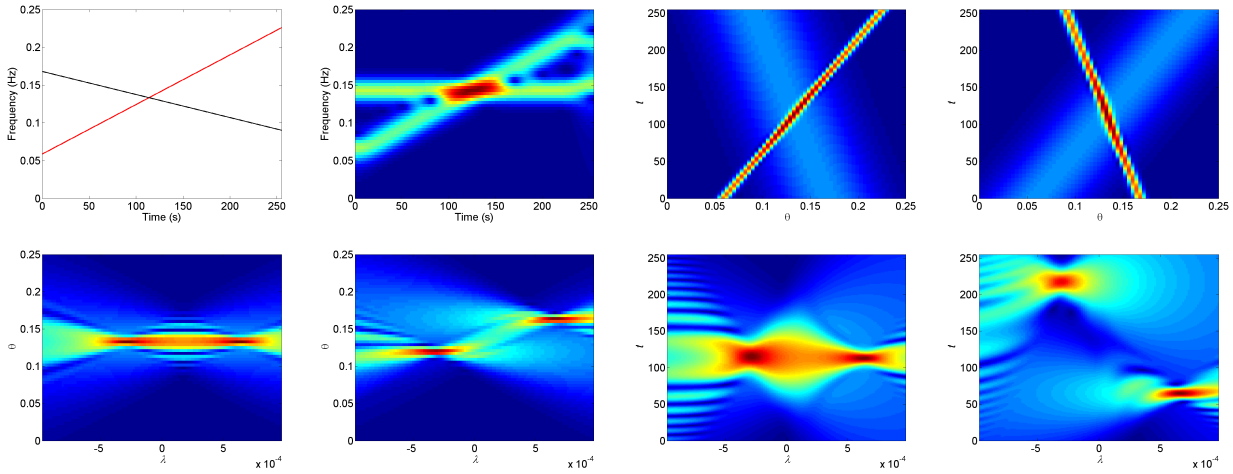

Figure 3: IFs, STFT, and some slices of the LQFT of the two-component signal $s(t)$ in (39). Top row (from left to right): IFs, STFT $|V_x(t,\eta)|$, $|\mathfrak{S}_s(t,\theta,r_1)|$ and $|\mathfrak{S}_s(t,\theta,r_2)|$; Bottom row (from left to right): $|\mathfrak{S}_s(114,\theta,\lambda)|$, $|\mathfrak{S}_s(160,\theta,\lambda)|$, $|\mathfrak{S}_s(t,c_2,\lambda)|$ and $|\mathfrak{S}_s(t,26/N,\lambda)|$.

To solve the above problem, we first consider the popular integral transform, namely Radon transform [61]. Since $\mathfrak{S}_s(t,\eta,\lambda)$ is a three dimensional function, we may use the 3D Radon transform as that in [62] to detect the signal components, which is similar to the case of two dimensional Radon transform in [63].

For each time t, with a pair of angles (φ_1, φ_2), the 3D Radon transform is an integral transform along the lines in the 3D space,

$$R(t', \varphi_1, \varphi_2) := \int_{-\infty}^{\infty}\int_{-\infty}^{\infty}\int_{-\infty}^{\infty} \mathfrak{S}_s(t,\eta,\lambda)\delta(t' - \eta\sin\varphi_1\cos\varphi_2 + \eta\sin\varphi_1\sin\varphi_2 + t\cos\varphi_1)dtd\eta d\lambda,$$

where δ is a Dirac's delta function.

If all the components of a multicomponent signal are LFM modes, then they can be well represented in the 3D space of $R(t', \varphi_1, \varphi_2)$. However, the computational burden is heavy for this 3D Radon transform. Moreover, a nonstationary signal is approximated to LFM mode just for local time around t.

Considering the relation among t, η and λ in $\mathfrak{S}_s(t,\eta,\lambda)$, namely $\phi'(t+u)=\eta+\lambda u, u\in[-b,b]$, where $b>0$ is small enough, we introduce a time-frequency filter operator $\mathcal{F}$ on $\mathfrak{S}_x$ to make different sub-signals more distinguishable in the LQFT space.

For a multicomponent signal $x(t)$, the time-frequency filter-matched LQFT (FLQFT) is defined by

$$\mathcal{F}^h\left(\mathfrak{S}_x\right)(t,\eta,\lambda):=\frac{1}{b}\int_{\mathbb{R}}h\big(\frac{u}{b}\big)\left|\mathfrak{S}_x(t+u,\eta+\lambda u,\lambda)\right|du, \tag{40}$$

where $h(t)$ is a fast decay window function with $h(t)\geq 0$ and $\int_{\mathbb{R}}h(t)dt=1$. In the following experiments, in order to simplify calculations, we will use a rectangular window with width of $2b$.

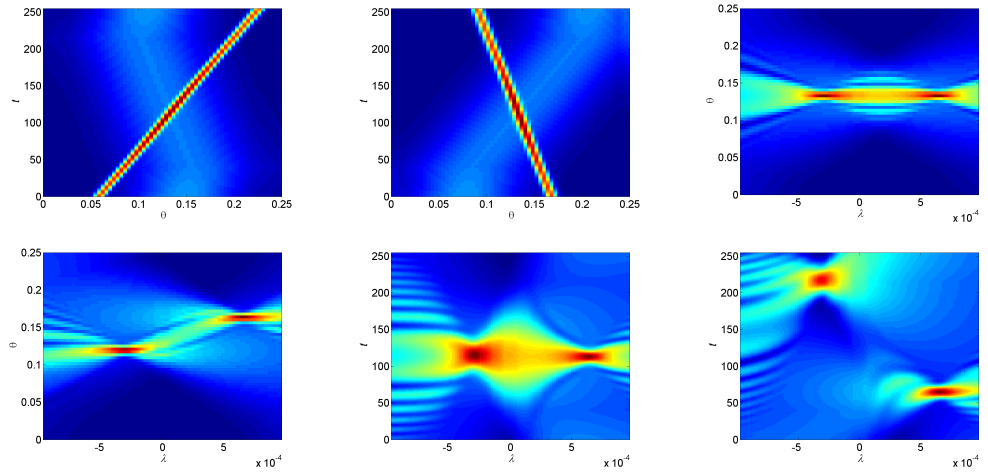

Figure 4: Slices of the FLQFT defined by (40) corresponding to the slices in Fig.3. Top row (from left to right): $|\mathcal{F}^h(\mathfrak{S}_s)(t,\theta,r_1)|$, $|\mathcal{F}^h(\mathfrak{S}_s)(t,\theta,r_2)|$ and $|\mathcal{F}^h(\mathfrak{S}_s)(114,\theta,\lambda)|$; Bottom row (from left to right): $|\mathcal{F}^h(\mathfrak{S}_s)(160,\theta,\lambda)|$, $|\mathcal{F}^h(\mathfrak{S}_s)(t,c_2,\lambda)|$ and $|\mathfrak{S}_s(t,26/N,\lambda)|$.

Consider again the two-component LFM signal in (39), Fig.4 shows the slices of the FLQFT defined by (40) with Gaussian window and $b=20$ (discrete points, unitless). Observe that by comparing the corresponding pictures in Fig.3 and Fig.4, FLQFT indeed improves the separability of the two components when their IFs are crossover.

For $x\in\mathcal{A}_\alpha$, we will use FLQFT to estimate $\phi'_\ell(t),\phi''_\ell(t)$ by

$$(\widehat{\eta}_\ell,\widehat{\lambda}_\ell):=\mathrm{argmax}_{\eta,\lambda\in\mathcal{G}_\ell}|\mathcal{F}^h(\mathfrak{S}_x)(t,\eta,\lambda)|, \tag{41}$$

where $\mathcal{G}_\ell$ is defined in Theorem 1. With the resulting $\widehat{\eta}_\ell,\widehat{\lambda}_\ell$, we may use LQFT (namely (32) or (33)) to recover sub-signal $x_\ell(t),1\leq\ell\leq K$. Observe that the recovering formula (32) or (33) recovers $x_\ell(t)$ one by one. Next, by considering all $x_\ell(t),0\leq\ell\leq K$ as a whole group, we propose an innovative algorithm based on LQFT to recover the sub-signals $x_\ell(t)$.

Recall that when g is the Gaussian window given in (24), then (37) holds. Thus for $x \in \mathcal{A}_\alpha$, we have

$$\mathfrak{S}_x(t,\eta,\lambda) \approx \sum_{\ell=0}^{K} x_\ell(t)\mathbb{A}(\lambda-\phi_\ell''(t))\Omega(\lambda-\phi_\ell''(t),\eta-\phi_\ell'(t)).$$

Hence if $\widehat{\eta}_\ell, \widehat{\lambda}_\ell, 1 \le \ell \le K$ obtained from FSSO by (41) are good approximations to $\phi_\ell'(t), \phi_\ell''(t)$, then, with $\widehat{\eta}_0 = \widehat{\lambda}_0 = 0$, we have

$$\mathfrak{S}_x(t,\eta,\lambda) \approx \sum_{\ell=0}^{K} x_\ell(t)\mathbb{A}(\lambda-\widehat{\lambda}_\ell)\Omega(\lambda-\widehat{\lambda}_\ell,\eta-\widehat{\eta}_\ell).$$

In particular, with $\eta = \widehat{\eta}_m, \lambda = \widehat{\lambda}_m$, we have

$$\mathfrak{S}_x(t,\widehat{\eta}_m,\widehat{\lambda}_m) \approx \sum_{\ell=0}^{K} a_{m,\ell}x_\ell(t), \quad m = 0,1,\cdots,K, \tag{42}$$

where

$$a_{m,\ell} := \mathbb{A}(\widehat{\lambda}_m-\widehat{\lambda}_\ell)\Omega(\widehat{\lambda}_m-\widehat{\lambda}_\ell,\widehat{\eta}_m-\widehat{\eta}_\ell). \tag{43}$$

Based on (42), we propose the following algorithm to recover components $x_\ell(t)$ and trend $x_0(t)$.

Algorithm 1. *(Signal reconstruction with improved LQFT). Let $x(t)$ be a multicomponent signal $x \in \mathcal{A}_\alpha$ satisfying (3) and $\mathfrak{S}_x(t,\eta,\lambda)$ be the LQFT of x with the Gaussian window function.*

Step 1. *Set $\widehat{\eta}_0 = \widehat{\lambda}_0 = 0$. Calculate $\widehat{\eta}_\ell, \widehat{\lambda}_\ell, 1 \le \ell \le K$ by (41), where $\mathcal{G}_\ell$ is defined in Theorem 1.*

Step 2. *Calculate*

$$\widetilde{\mathbf{X}}_t := \mathbf{A}^{-1}\widehat{\mathbf{X}}_t = \begin{bmatrix} 1 & a_{0,1} & \cdots & a_{0,K} \\ a_{1,0} & 1 & \cdots & a_{1,K} \\ \vdots & \vdots & \ddots & \vdots \\ a_{K,0} & a_{K,1} & \cdots & 1 \end{bmatrix}^{-1} \widehat{\mathbf{X}}_t, \tag{44}$$

where $\widehat{\mathbf{X}}_t := [\widehat{x}_0(t), \widehat{x}_1(t), \cdots, \widehat{x}_K(t)]^T$ with $\widehat{x}_\ell(t) = \mathfrak{S}_x(t,\widehat{\eta}_\ell,\widehat{\lambda}_\ell)$, $a_{m,\ell}$ are defined by (43) and $\mathbf{A} = [a_{m,\ell}]_{0\le m,\ell\le K}$.

Step 3. *The components $\widetilde{x}_\ell(t)$ of $\widetilde{\mathbf{X}}_t =: [\widetilde{x}_0(t), \widetilde{x}_1(t), \cdots, \widetilde{x}_K(t)]^T$ are the recovered sub-signals $x_\ell(t)$ of $x(t)$.*

Note that $\Omega(r,\eta)$ is a fast decay function with respect to η. If the IF of sub-signal $x_m(t)$ is well-separated (satisfying (2)) from other signals' IF, then we have $a_{\ell,m} \approx 0$ for $\ell \ne m$. Furthermore, if all the sub-signals $\mathbf{X}_t$ are well-separated in the time-frequency plane, namely satisfy (2), then $\mathbf{A}$ in (44) is essentially the identity matrix. So the reconstruction algorithm above is fit for both cases in (2) and (3).

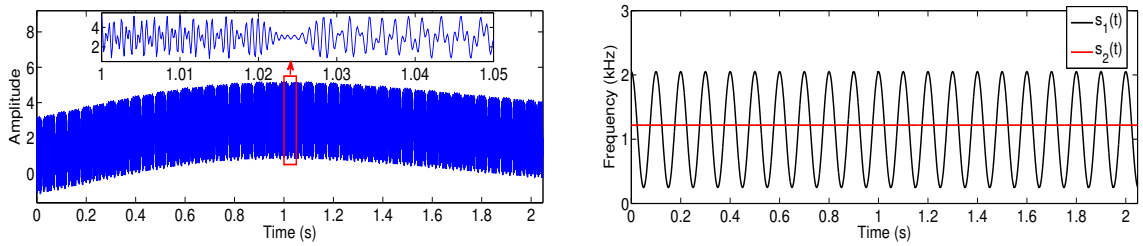

Figure 5: The waveform of $s(t)$ in (45) with enlarged picture around $t = 1$ (Left) and the IFs of two AM-FM components (Right).

Finally, we discuss the algorithm of real-time processing of an consecutive input signal. To reduce the computational cost, we need to predefine some variables. Let $T \in \mathbb{Z}^+$ denote the truncation length of the input signal, e.g. $T = 128$ or $T = 256$, then frequency η is discretized into $\eta = 0, 1/T, ..., (T/2-1)/T$ and λ is discretized into $\lambda = -(T/2-1)/T^2, -(T/2-2)/T, ..., 0, ...(T/2-1)/T^2$. Define $\mathbf{S}^{t_m}_{T/2\times(T-1)} = \mathfrak{S}_x(t_m, \cdot, \cdot)$, where t_m is a fixed time. Suppose we will separate x when $t = t_m$, then we need to calculate $\mathbf{S}^{t_m-M}, \cdots, \mathbf{S}^{t_m+M}$ first, where $2M+1$ should equivalent to the window length b in (40) and $2M+1 \ll T$. Then for the next time instant $t = t_m + 1$, we just need to calculate $\mathbf{S}^{t_m+1+M}$, and continue the procedure.

4 Numerical experiments

Fig.2 demonstrates our proposed method (Algorithm 1) is efficient for the two-component signal in (13) with one cross point of the IFs. In this section, we first consider another synthetic multicomponent signal $s(t)$, given as

$$\begin{aligned} s(t) &= s_1(t) + s_2(t) + A_0(t) \\ &= 1.2\cos\big(2300\pi t + 90\sin(20\pi t)\big) + \cos\big(2438\pi t\big) + \big(1 + (t^2+t)e^{1-t^{1.5}}\big), \end{aligned} \tag{45}$$

where $t > 0$. Note that the IFs of $s_1(t)$ and $s_2(t)$ are $\phi_1'(t) = 1150+900\cos(20\pi t)$ and $\phi_2'(t) = 1219$, respectively, called IF1 and IF2 in Fig.6.

In this experiment, we discretize $s(t)$ with a sampling rate $F_s = 8$kHz and data length $N = 2^{14}$, namely $t \in [0, 2.048]$. Fig.5 shows the waveform of $s(t)$ and the IFs of two AM-FM components, $s_1(t)$ and $s_2(t)$. As the expression in (45), $s(t)$ consists of one trend and two oscillating AM-FM components. Meanwhile, the IFs of the two AM-FM components are crossover.

Observe that the signal $s(t)$ to be processed contains lots of samples, which should be analyzed or separated locally. Here we use a sliding truncated Gaussian window with length of $N = 2^8$ points for methods of STFT, SST and LQFT. Hence the frequency bins is discretized as $\frac{F_s}{N}\{-N/2+1, -N/2+2, ..., N/2-1, N/2\}$ for complex signals, or just $\frac{F_s}{N}\{0, 1, ..., N/2-1, N/2\}$

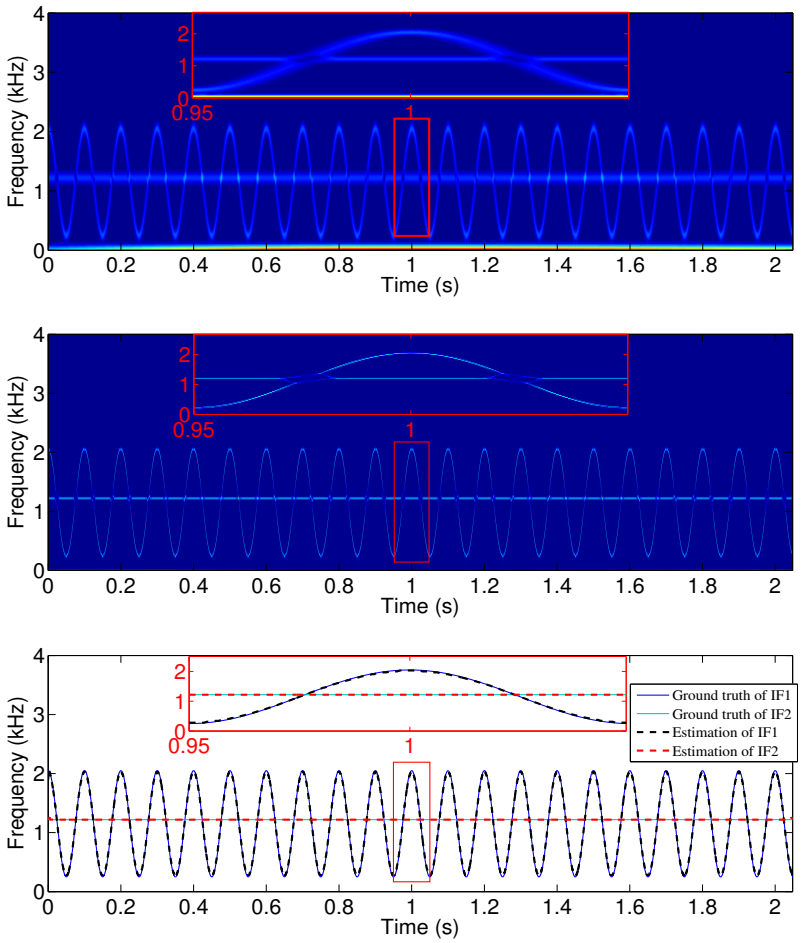

Figure 6: Recovered IFs of $s(t)$ in (45) with SST and LQFT (with enlarged picture around $t = 1$). Top: Time-frequency diagram of STFT; Middle: Time-frequency diagram of the second-order SST in [39]; Bottom: recovered IFs with Algorithm 1.

for real signals. Note that we set N as a power of 2 to take full advantage of the fast Fourier transform. Fig.6 shows some of the experimental results of SST and LQFT. The enlarged pictures around $t = 1$ are also attached with each sub-figure. Obviously, when the IFs of $s_1(t)$ and $s_2(t)$ are crossover, either the STFT or the 2nd-order FSST hardly represents the sub-signals reliably. Thus we cannot use the time-frequency diagram of STFT or the 2nd-order FSST to extract the IFs of the sub-signals for the purpose of recovering their waveforms. However, using our LQFT method, we can extract the IFs of $s(t)$ accurately.

Fig.7 provides the recovered waveforms with Algorithm 1 proposed in §3.2. Since there are so many sample periods of the signal $s(t)$, we just show a small truncation around $t = 1$. Observe the differences between the recovered waveforms and the truth ones are extremely small. Since the existing signal decomposition methods based on EMD or SST cannot solve the IF crossover

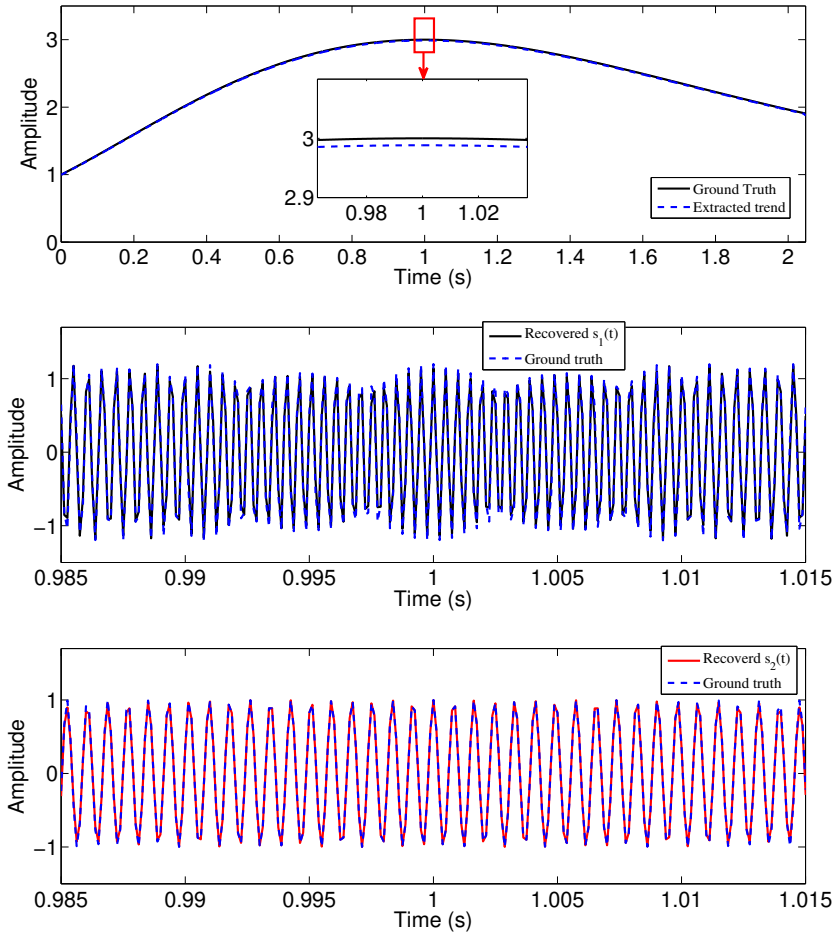

Figure 7: Recovery results of $s(t)$ in (45) with the proposed Algorithm 1. Top: the recovered trend with enlarged picture around $t = 1$; Middle: signal component $s_1(t)$; Bottom: signal component $s_2(t)$.

problem, we will not provide the recovery results of those methods here.

Finally, we consider a real signal, the radar echoes. Fig.8 shows the waveform and spectrum of the radar echoes. Note that the sampling rate here is equal to 400 Hz, which is just the pulse repetition frequency of the radar. The bottom panel of Fig.8, namely the spectrum shows that this signal consists of several broadband components and a trend.

Fig.9 shows some results of the radar echoes in Fig.8. From their STFTs (top-left panel in Fig.9), there are two components (two radar targets) in the echoes. Meanwhile, the IF curves of these two targets are crossover with the trend component. Although the 2nd-order SST can squeeze the time-frequency plane of STFT, it is still affected by the trend component when they are crossover. The top-right panel of Fig.9 shows a specific slice of the 3D LQFT matrix, where the chirp rate is approximately equal to the average chirp rate of Component 1 and Component 2. Observe that the trend component is weakened in the specific slice. The results demonstrate

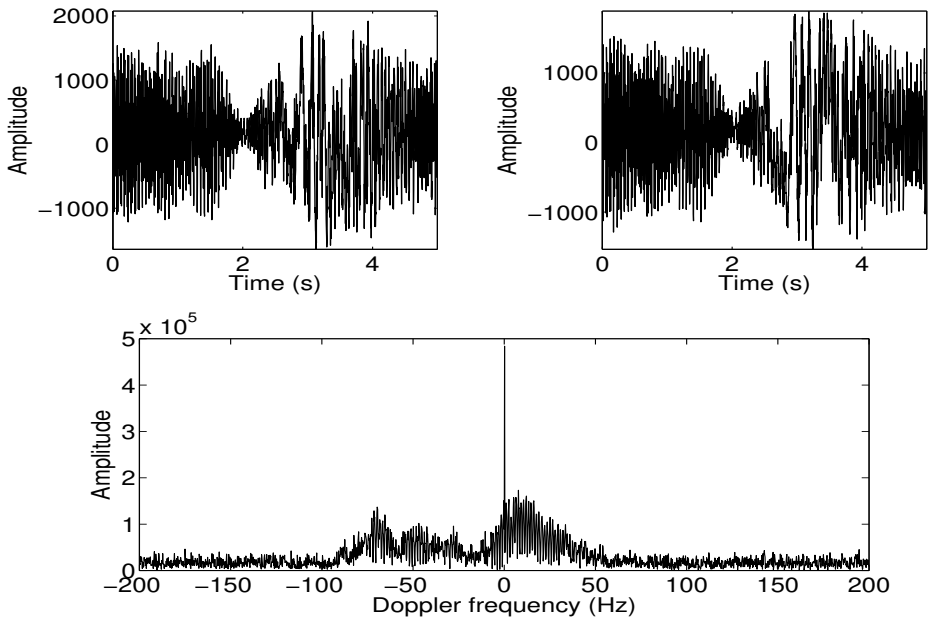

Figure 8: Waveform and spectrum of the radar echoes. Top-left: the real part of the waveform; Top-right: the imaginary part of the waveform; Bottom: the spectrum.

the proposed method in this paper is efficient in separating multicomponent with crossover IF curves.

5 Conclusions

In this paper, we propose the localized quadratic-phase Fourier transform (LQFT) for multicomponent signal separation with crossover instantaneous frequencies. We define the modified adaptive harmonic model and the conditions to represent crossover components separately by LQFT. The error bounds for instantaneous frequency estimation and sub-signal recovery are provided. Based on the approximation of source signals with linear frequency modulation (LFM) modes at any local time, we propose an improved signal reconstruction algorithm. The numerical experiments demonstrate the proposed method are more accurate and consistent in signal separation than EMD, SST and other approaches. The proposed method has a great potential for a variety of engineering applications such as channel detection in communication, fault monitoring in mechanical systems etc.

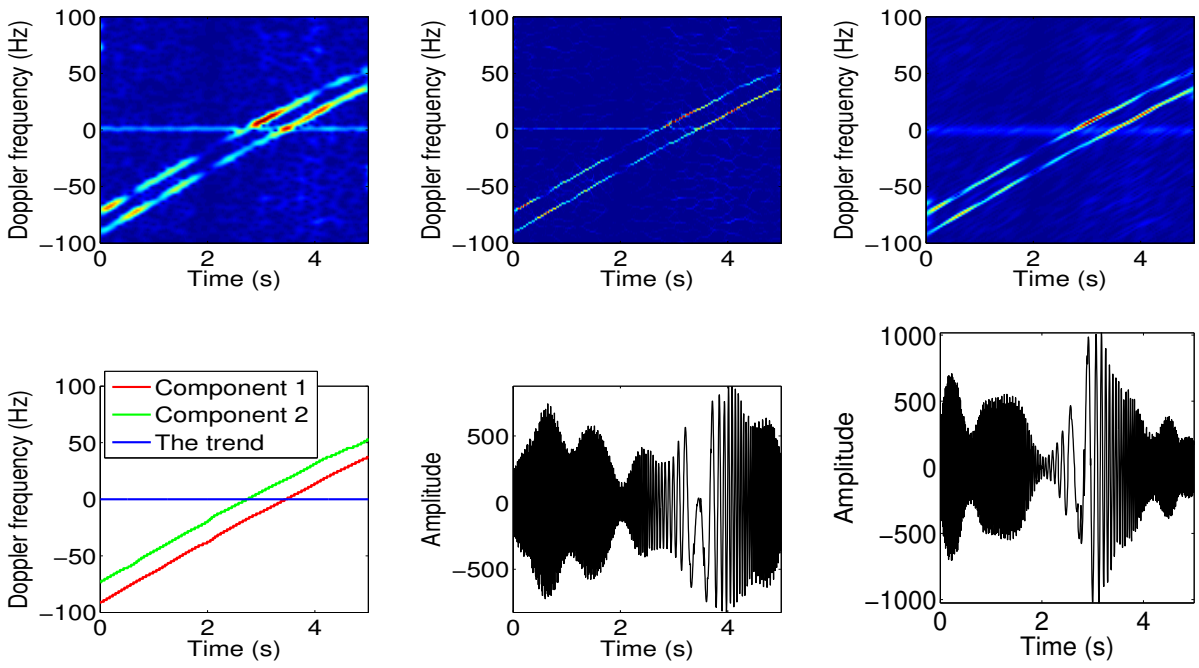

Figure 9: Results of the radar echoes. Top row (from left to right): STFT, 2nd-order SST, a specific slice of the 3D LQFT matrix; Bottom row (from left to right): the estimated IFs by the proposed method, the recovered waveform of Component 1 (real part) and the recovered waveform of Component 2 (real part).

Appendix

In this appendix we provide the proof of Theorem 1. Write

$$x(t+\tau) = x_{\rm m}(t,\tau) + x_{\rm r}(t,\tau),$$

where

$$\begin{aligned} x_{\rm m}(t,\tau) &:= \sum_{k=0}^{K} x_k(t) e^{i2\pi(\phi_k'(t)\tau + \frac{1}{2}\phi_k''(t)\tau^2)}, \\ x_{\rm r}(t,\tau) &:= \sum_{k=0}^{K} \Big\{ (A_k(t+\tau) - A_k(t)) e^{i2\pi\phi_k(t+\tau)} \\ &\qquad + x_k(t) e^{i2\pi(\phi_k'(t)\tau + \frac{1}{2}\phi_k''(t)\tau^2)} \big(e^{i2\pi(\phi_k(t+\tau) - \phi_k(t) - \phi_k'(t)\tau - \frac{1}{2}\phi_k''(t)\tau^2)} - 1 \big) \Big\}. \end{aligned}$$

Denote

$$\mathfrak{R}_x(t,\eta,\lambda) := \int_{\mathbb{R}} x_{\rm m}(t,\tau) \mathcal{K}_\sigma(\tau,\eta,\lambda) d\tau = \int_{\mathbb{R}} \frac{1}{\sigma} g\big(\frac{\tau}{\sigma}\big) x_{\rm m}(t,\tau) e^{-i2\pi\tau\eta - i\pi\lambda\tau^2} d\tau. \tag{46}$$

Then we have

$$\mathfrak{R}_x(t,\eta,\lambda) = \sum_{k=0}^{K} x_k(t)\, \breve{g}\left(\sigma(\eta - \phi_k'(t)), \sigma^2(\lambda - \phi_k''(t))\right). \tag{47}$$

In following, $\sigma = \frac{c_0}{\alpha^2}$ as in Theorem 1. In addition, since in general α is small, we assume $\sigma \geq 1$ for simplicity of presentation. Furthermore, since x, t will be fixed throughout the proof, in the following we use $\mathfrak{S}(\eta,\lambda)$, $\mathfrak{R}(\eta,\lambda)$, $\mathcal{G}$ and $\mathcal{G}_\ell$ to denote $\mathfrak{S}_x(t,\eta,\lambda)$, $\mathfrak{R}_x(t,\eta,\lambda)$, $\mathcal{G}(t)$ and $\mathcal{G}_\ell(t)$ respectively. First we establish a few lemmas.

Lemma 1. *For $x(t) \in A_\alpha$, let $x_{\rm m}(t,\tau)$ be the LFM approximation to $x(t+\tau)$ at time t defined above. Then*

$$|x(t+\tau) - x_{\rm m}(t,\tau)| \leq M\big(B_1\alpha^3|\tau| + \frac{\pi}{3}B_2\alpha^7|\tau|^3\big). \tag{48}$$

Proof. The proof is straightforward. Indeed, by (17) and (18),

$$\begin{aligned}
&|x(t+\tau) - x_{\rm m}(t,\tau)| = |x_{\rm r}(t,\tau)| \\
&\leq \sum_{k=0}^{K}\Big\{|A_k(t+\tau) - A_k(t)| + A_k(t)\ \big|i2\pi\big(\phi_k(t+\tau) - \phi_k(t) - \phi_k'(t)\tau - \frac{1}{2}\phi_k''(t)\tau^2\big)\big|\Big\} \\
&\leq \sum_{k=0}^{K}\Big\{A_k(t)B_1\alpha^3|\tau| + A_k(t)2\pi\sup_{\xi\in\mathbb{R}}\frac{1}{6}\big|\phi'''_k(\xi)\tau^3\big| \\
&\leq M(t)B_1\alpha^3|\tau| + \sum_{k=0}^{K}A_k(t)\frac{\pi}{3}B_2\alpha^7|\tau|^3 = M\big(B_1\alpha^3|\tau| + \frac{\pi}{3}B_2\alpha^7|\tau|^3\big),
\end{aligned}$$

as desired. □

Lemma 2. *For $x(t) \in A_\alpha$, let $\mathfrak{S}(\eta,\lambda)$ be its transform by LQFT and $\mathfrak{R}(\eta,\lambda)$ be the approximation of $\mathfrak{S}(\eta,\lambda)$ with LFMs defined by* (46)*. Then*

$$\big|\mathfrak{S}(\eta,\lambda) - \mathfrak{R}(\eta,\lambda)\big| \leq \alpha M\big(B_1c_0N + \frac{\pi}{3}B_2c_0^3N^3\big). \tag{49}$$

Proof. By (48) and the facts $g \geq 0$, supp$g \subseteq [-N,N]$, we have

$$\begin{aligned}
\big|\mathfrak{S}(\eta,\lambda) - \mathfrak{R}(\eta,\lambda)\big| &= \Big|\int_{\mathbb{R}}(x(t+\tau) - x_{\rm m}(t,\tau))\frac{1}{\sigma}g(\frac{\tau}{\sigma})e^{-i2\pi(\eta\tau+\frac{1}{2}\lambda\tau^2)}d\tau\Big| \\
&\leq \int_{-N\sigma}^{N\sigma}M\big(B_1\alpha^3|\tau| + \frac{\pi}{3}B_2\alpha^7|\tau|^3\big)\frac{1}{\sigma}g(\frac{\tau}{\sigma})d\tau \\
&\leq M\big(B_1\alpha^3N\sigma + \frac{\pi}{3}B_2\alpha^7\sigma^3N^3\big) = \alpha M\big(B_1c_0N + \frac{\pi}{3}B_2c_0^3N^3\big).
\end{aligned}$$

□

Lemma 3. *Let $\mathcal{G}_\ell, 0 \leq \ell \leq K$ be the sets defined by* (28)*. If $\alpha \leq \frac{\mu\sqrt{c_0\triangle}}{4ML}$, then $\mathcal{G}_\ell$ are nonoverlapping, namely, $\mathcal{G}_\ell \cap \mathcal{G}_k = \emptyset$ for $\ell \neq k$.*

Proof. Assume $(\eta,\lambda)\in\mathcal{G}_\ell\cap\mathcal{G}_k$ for some $\ell\neq k$. By the definition of $\mathcal{G}_\ell$, we have

$$\begin{aligned}
&|\phi_k'(t)-\phi_\ell'(t)|+\rho|\phi_k''(t)-\phi_\ell''(t)|\\
&\le |\phi_k'(t)-\eta|+\rho|\phi_k''(t)-\lambda|+|\phi_\ell'(t)-\eta|+\rho|\phi_\ell''(t)-\lambda|\\
&\le \frac{1}{\sigma}\left(\sigma|\phi_k'(t)-\eta|+\rho\sigma^2|\phi_k''(t)-\lambda|\right)+\frac{1}{\sigma}\left(\sigma|\phi_\ell'(t)-\eta|+\rho\sigma^2|\phi_\ell''(t)-\lambda|\right)\quad(\text{since }\sigma\ge 1)\\
&\le \frac{2}{\sigma}\Big(\frac{4ML}{\mu}\Big)^2\le 2\triangle,
\end{aligned}$$

a contradiction to the well-separated condition (3). Thus the sets $\mathcal{G}_\ell, 0\le\ell\le K$ are nonoverlapping. □

Since we assume $\sigma\ge 1$, from (3), we have

$$\begin{aligned}
&\sigma|\phi_k'(t)-\phi_\ell'(t)|+\rho\,\sigma^2|\phi_k''(t)-\phi_\ell''(t)|\\
&\ge \sigma\Big(|\phi_k'(t)-\phi_\ell'(t)|+\rho|\phi_k''(t)-\phi_\ell''(t)|\\
&\ge 2\sigma\triangle.
\end{aligned}\tag{50}$$

Lemma 4. *For $x(t)\in A_\alpha$, let $\mathfrak{R}(\eta,\lambda)$ be defined by (46). If $\sigma\triangle\ge\left(\frac{4ML}{\mu}\right)^2$, that is $\alpha\le\frac{\mu\sqrt{c_0\triangle}}{4ML}$ when $\sigma=\frac{c_0}{\alpha^2}$, then*

$$\left|\mathfrak{R}(\eta,\lambda)-x_\ell(t)\,\breve{g}\left(\sigma(\eta-\phi_\ell'(t)),\sigma^2(\lambda-\phi_\ell''(t))\right)\right|\le\frac{ML}{\sqrt{\sigma\triangle}},\forall(\eta,\lambda)\in\mathcal{G}_\ell,\tag{51}$$

$$\left|\mathfrak{R}(\phi_\ell'(t),\phi_\ell''(t))-x_\ell(t)\right|\le\frac{ML}{\sqrt{2\sigma\triangle}}.\tag{52}$$

Proof. By (47), we have for any $(\eta,\lambda)\in\mathcal{G}_\ell$,

$$\begin{aligned}
&\left|\mathfrak{R}(\eta,\lambda)-x_\ell(t)\,\breve{g}\left(\sigma(\eta-\phi_\ell'(t)),\sigma^2(\lambda-\phi_\ell''(t))\right)\right|\\
&=\Big|\sum_{k\neq\ell}x_k(t)\,\breve{g}\left(\sigma(\eta-\phi_k'(t)),\sigma^2(\lambda-\phi_k''(t))\right)\Big|\\
&\le\sum_{k\neq\ell}A_k(t)L\big(\sigma|\eta-\phi_k'(t)|+\rho\sigma^2|\lambda-\phi_k''(t)|\big)^{-\frac{1}{2}}\quad(\text{by (21)})\\
&\le\sum_{k\neq\ell}A_k(t)L\big(\sigma|\phi_\ell'(t)-\phi_k'(t)|-\sigma|\eta-\phi_\ell'(t)|+\rho\sigma^2|\phi_\ell''(t)-\phi_k''(t)|-\rho\sigma^2|\lambda-\phi_\ell''(t)|\big)^{-\frac{1}{2}}\\
&\le\sum_{k\neq\ell}A_k(t)L\big(2\sigma\triangle-\big(\frac{4ML}{\mu}\big)^2\big)^{-\frac{1}{2}}\quad(\text{by (50) and (28)})\\
&\le\frac{ML}{\sqrt{\sigma\triangle}},
\end{aligned}$$

since $\sigma\triangle\ge\left(\frac{4ML}{\mu}\right)^2$. This proves (51). The proof (52) is similar and the details are omitted. □

Proof of Theorem (a). Let $(\eta,\lambda)\in\mathcal{G}$. Suppose $(\eta,\lambda)\notin G_\ell$ for any ℓ. Then

$$\sigma|\eta-\phi_k'(t)|+\rho\sigma^2|\lambda-\phi_k''(t)|>\big(\frac{4ML}{\mu}\big)^2.$$

Hence,

$$\begin{aligned}\big|\mathfrak{R}(\eta,\lambda)\big|&=\Big|\sum_{k=0}^{K}x_k(t)\,\breve{g}\left(\sigma(\eta-\phi_k'(t)),\sigma^2(\lambda-\phi_k''(t))\right)\Big|\\&\le\sum_{k=0}^{K}A_k(t)\frac{L}{\big(\sigma|\eta-\phi_k'(t)|+\sigma^2|\lambda-\phi_k''(t)|\big)^{\frac{1}{2}}}\quad\text{(by (21))}\\&<\sum_{k=0}^{K}\frac{A_k(t)L}{4ML/\mu}=\frac{\mu}{4}.\end{aligned}$$

This, together with (49), implies

$$\begin{aligned}\big|\mathfrak{S}(\eta,\lambda)\big|&\le\big|\mathfrak{S}(\eta,\lambda)-\mathfrak{R}(\eta,\lambda)\big|+\big|\mathfrak{R}(\eta,\lambda)\big|\\&\le\alpha M\big(B_1c_0N+\frac{\pi}{3}B_2c_0^3N^3\big)+\frac{\mu}{4}\\&\le\frac{\mu}{4}+\frac{\mu}{4}=\frac{\mu}{2},\end{aligned}$$

where the second last inequality follows (27) on the condition for α. This leads to a contradiction that $(\eta,\lambda)\in\mathcal{G}$. Hence there must exist ℓ such that $(\eta,\lambda)\in\mathcal{G}_\ell$. Lemma 3 has shown that $\mathcal{G}_\ell, 0\le\ell\le K$ are disjoint.

Finally we show that each $\mathcal{G}_\ell$ is non-empty. To this regard, we show $(\phi_\ell'(t),\phi_\ell''(t))\in\mathcal{G}$. Indeed, the following fact followed from (52)

$$\big|\mathfrak{R}(\phi_\ell'(t),\phi_\ell''(t))\big|\ge|x_\ell(t)|-\frac{ML}{\sqrt{2\sigma\triangle}}\ge\mu-\frac{\mu}{4\sqrt{2}}>\frac{3\mu}{4}$$

implies

$$\begin{aligned}\big|\mathfrak{S}(\phi_\ell'(t),\phi_\ell''(t))\big|&\ge\big|\mathfrak{R}(\phi_\ell'(t),\phi_\ell''(t))\big|-\big|\mathfrak{S}(\phi_\ell'(t),\phi_\ell''(t))-\mathfrak{R}(\phi_\ell'(t),\phi_\ell''(t))\big|\\&>\frac{3\mu}{4}-\frac{\mu}{4}=\frac{\mu}{2}.\end{aligned}$$

Hence $(\phi_\ell'(t),\phi_\ell''(t))\in\mathcal{G}$. □

Proof of (29)**.** By the definition of $\widehat{\eta}_\ell$ and $\widehat{\lambda}_\ell$, (49) and (52), we have

$$\begin{aligned}&|\mathfrak{S}(\widehat{\eta}_\ell,\widehat{\lambda}_\ell)|\ge|\mathfrak{S}(\phi_\ell'(t),\phi_\ell''(t))|\\&\ge|\mathfrak{R}(\phi_\ell'(t),\phi_\ell''(t))|-\alpha M\big(c_0NB_1+\frac{\pi}{3}B_2c_0^3N^3\big)\\&\ge A_\ell(t)-\frac{LM}{\sqrt{2\sigma\triangle}}-\alpha M\big(c_0NB_1+\frac{\pi}{3}B_2c_0^3N^3\big)\\&\ge A_\ell(t)-\alpha M\Big(\frac{L}{\sqrt{c_0\triangle}}+c_0NB_1+\frac{\pi}{3}B_2c_0^3N^3\Big).\end{aligned}\tag{53}$$

On the other hand, by (49) and (51), we have

$$
\begin{aligned}
&|\mathfrak{S}(\widehat{\eta}_\ell,\widehat{\lambda}_\ell)| \le |\mathfrak{R}(\widehat{\eta}_\ell,\widehat{\lambda}_\ell)| + \alpha M\big(c_0NB_1+\frac{\pi}{3}B_2c_0^3N^3\big)\\
&\le |x_\ell(t)\,\breve{g}\,\big(\sigma(\widehat{\eta}_\ell-\phi'_\ell(t)),\sigma^2(\widehat{\lambda}_\ell-\phi''_\ell(t))\big)\big| + \frac{LM}{\sqrt{\sigma\triangle}} + \alpha M\big(c_0NB_1+\frac{\pi}{3}B_2c_0^3N^3\big)\\
&\le A_\ell(t) + \alpha M\Big(\frac{L}{\sqrt{c_0\triangle}} + c_0NB_1+\frac{\pi}{3}B_2c_0^3N^3\Big)\ \ (\text{since } |\,\breve{g}(\eta,\lambda)|\le 1). \qquad (54)
\end{aligned}
$$

Relationship of $|\mathfrak{S}(\widehat{\eta}_\ell,\widehat{\lambda}_\ell)|$ and $A_\ell(t)$ in (53) and (54) leads to (29). □

Proof of (30)**.** Write $\mathfrak{S}(\widehat{\eta}_\ell,\widehat{\lambda}_\ell) = |\mathfrak{S}(\widehat{\eta}_\ell,\widehat{\lambda}_\ell)|e^{i2\pi\psi(t)}$ for some real-valued function $\psi(t)$. Since for any complex number z_1, z_2, $\big||z_1|-|z_2|\big| \le |z_1-z_2|$, we have

$$
\begin{aligned}
&A_\ell(t)\big|\,|\,\breve{g}\,\big(\sigma(\widehat{\eta}_\ell-\phi'_\ell(t)),\sigma^2(\widehat{\lambda}_\ell-\phi''_\ell(t))\big)| - 1\big|\\
&\le A_\ell(t)\big|\,\breve{g}\,\big(\sigma(\widehat{\eta}_\ell-\phi'_\ell(t)),\sigma^2(\widehat{\lambda}_\ell-\phi''_\ell(t))\big)e^{i2\pi\phi_\ell(t)} - e^{-i2\pi\psi(t)}\big|\\
&= \big|\,\breve{g}\,\big(\sigma(\widehat{\eta}_\ell-\phi'_\ell(t)),\sigma^2(\widehat{\lambda}_\ell-\phi''_\ell(t))\big)x_\ell(t) - A_\ell(t)e^{-i2\pi\psi(t)}\big|\\
&\le \big|\,\breve{g}\,\big(\sigma(\widehat{\eta}_\ell-\phi'_\ell(t)),\sigma^2(\widehat{\lambda}_\ell-\phi''_\ell(t))\big)x_\ell(t) - \mathfrak{S}(\widehat{\eta}_\ell,\widehat{\lambda}_\ell)\big| + \big|\mathfrak{S}(\widehat{\eta}_\ell,\widehat{\lambda}_\ell) - A_\ell(t)e^{-i2\pi\psi(t)}\big|\\
&\le \big|\,\breve{g}\,\big(\sigma(\widehat{\eta}_\ell-\phi'_\ell(t)),\sigma^2(\widehat{\lambda}_\ell-\phi''_\ell(t))\big)x_\ell(t) - \mathfrak{R}(\widehat{\eta}_\ell,\widehat{\lambda}_\ell)\big| + \big|\mathfrak{S}(\widehat{\eta}_\ell,\widehat{\lambda}_\ell) - \mathfrak{R}(\widehat{\eta}_\ell,\widehat{\lambda}_\ell)\big| + \big||\mathfrak{S}(\widehat{\eta}_\ell,\widehat{\lambda}_\ell)| - A_\ell(t)\big|\\
&\le \frac{ML}{\sqrt{\sigma\triangle}} + \alpha M\big(c_0NB_1+\frac{\pi}{3}MB_2c_0^3N^3\big) + \alpha M\big(\frac{L}{\sqrt{c_0\triangle}} + c_0NB_1+\frac{\pi}{3}B_2c_0^3N^3\big)\\
&= 2\alpha M\big(\frac{L}{\sqrt{c_0\triangle}} + c_0NB_1+\frac{\pi}{3}B_2c_0^3N^3\big),
\end{aligned}
$$

where the second inequality follows from (51), (49), and (29). Thus $\breve{g}$ satisfies (22) with $\eta = \sigma(\widehat{\eta}_\ell-\phi'_\ell(t)), \lambda = \sigma^2(\widehat{\lambda}_\ell-\phi''_\ell(t)$ and $\varepsilon=\alpha$. Hence (30) holds by the property (b) of the admissible window function g. □

Proof of (31)**.** By (49) and (52), we have

$$
\begin{aligned}
&\big|\mathfrak{S}(\widehat{\eta}_\ell,\widehat{\lambda}_\ell) - x_\ell(t)\big|\\
&\le \big|\mathfrak{S}(\widehat{\eta}_\ell,\widehat{\lambda}_\ell) - \mathfrak{S}(\phi'_\ell(t),\phi''_\ell(t))\big| + \big|\mathfrak{S}(\phi'_\ell(t),\phi''_\ell(t)) - \mathfrak{R}(\phi'_\ell(t),\phi''_\ell(t))\big| + \big|\mathfrak{R}(\phi'_\ell(t),\phi''_\ell(t)) - x_\ell(t)\big|\\
&\le \Big|\frac{1}{\sigma}\int_{\mathbb{R}} g(\frac{\tau}{\sigma})\big(e^{-i2\pi\widehat{\eta}_\ell\tau - i\pi\widehat{\lambda}_\ell\tau^2} - e^{-i2\pi\widehat{\phi}'_\ell(t)\tau - i\pi\widehat{\phi}''_\ell(t)\tau^2}\big)d\tau\Big| + \alpha M\big(c_0NB_1+\frac{\pi}{3}B_2c_0^3N^3\big) + \frac{LM}{\sqrt{\sigma\triangle}}\\
&\le \frac{1}{\sigma}\int_{\mathbb{R}} g(\frac{\tau}{\sigma})\big|2\pi\widehat{\eta}_\ell\tau + \pi\widehat{\lambda}_\ell\tau^2 - 2\pi\phi'_\ell(t)\tau - \pi\phi''_\ell(t)\tau^2\big|d\tau + \alpha M\Big(\frac{L}{\sqrt{c_0\triangle}} + c_0NB_1+\frac{\pi}{3}B_2c_0^3N^3\Big)\\
&\le 2\pi|\widehat{\eta}_\ell-\phi'_\ell(t)|\frac{1}{\sigma}\int_{\mathbb{R}} g(\frac{\tau}{\sigma})|\tau|d\tau + \pi|\widehat{\lambda}_\ell-\phi''_\ell(t)|\frac{1}{\sigma}\int_{\mathbb{R}} g(\frac{\tau}{\sigma})\tau^2 d\tau + \alpha M\Big(\frac{L}{\sqrt{c_0\triangle}} + c_0NB_1+\frac{\pi}{3}B_2c_0^3N^3\Big)\\
&\le 2\pi|\widehat{\eta}_\ell-\phi'_\ell(t)\sigma N + \pi|\widehat{\lambda}_\ell-\phi''_\ell(t)|\sigma^2N^2 + \alpha M\Big(\frac{L}{\sqrt{c_0\triangle}} + c_0NB_1+\frac{\pi}{3}B_2c_0^3N^3\Big)\\
&= o(1) + \alpha M\Big(\frac{L}{\sqrt{c_0\triangle}} + c_0NB_1+\frac{\pi}{3}B_2c_0^3N^3\Big),
\end{aligned}
$$

where the last equality follows from (30). This completes the proof of (31). □

References

[1] N.E. Huang, Z. Shen, S.R. Long, M.L. Wu, H.H. Shih, Q. Zheng, N.C. Yen, C.C. Tung, and H.H. Liu, "The empirical mode decomposition and Hilbert spectrum for nonlinear and nonstationary time series analysis," *Proc. Roy. Soc. London A*, vol. 454, no. 1971, pp. 903–995, Mar. 1998.

[2] P. Flandrin, G. Rilling, and P. Goncalves, "Empirical mode decomposition as a filter bank," *IEEE Signal Proc. Letters*, vol. 11, no. 2, pp. 112–114, Feb. 2004.

[3] N. Ur Rehman and D. P. Mandic, "Filter bank property of multivariate empirical mode decomposition," *IEEE Trans. Signal Proc.*, vol. 59, no. 5, pp. 2421-2426, May 2011.

[4] G. Rilling and P. Flandrin, "One or two frequencies? The empirical mode decomposition answers," *IEEE Trans. Signal Proc.*, vol. 56, pp. 85–95, Jan. 2008.

[5] Z. Wu and N. E. Huang, "Ensemble empirical mode decomposition: A noise-assisted data analysis method," *Adv. Adapt. Data Anal.*, vol. 1, no. 1, pp. 1–41, Jan. 2009.

[6] Y. Xu, B. Liu, J. Liu, and S. Riemenschneider, "Two-dimensional empirical mode decomposition by finite elements," *Proc. Roy. Soc. London A*, vol. 462, no. 2074, pp. 3081–3096, Oct. 2006.

[7] N. Ur Rehman and D.P. Mandic, "Empirical mode decomposition for trivariate signals," *IEEE Trans. Signal Proc.*, vol. 58, no. 3, pp. 1059-68, Mar. 2010.

[8] T. Oberlin, S. Meignen, and V. Perrier, "An alternative formulation for the empirical mode decomposition," *IEEE Trans. Signal Proc.*, vol. 60, no. 5, pp. 2236–2246, May 2012.

[9] Y. Wang, G.-W. Wei and S.Y. Yang , "Iterative filtering decomposition based on local spectral evolution kernel," *J. Scientific Computing*, vol. 50, no. 3, pp. 629–664, Mar. 2012.

[10] A. Cicone, J.F. Liu, and H.M. Zhou, "Adaptive local iterative filtering for signal decomposition and instantaneous frequency analysis," *Appl. Comput. Harmon. Anal.*, vol. 41, no. 2, pp. 384–411, Sep. 2016.

[11] J. Gilles, "Empirical wavelet transform," *IEEE Trans. Signal Proc.*, vol. 61, no. 16, pp. 3999-4010, Aug. 2013.

[12] L. Li and H. Cai, Q. Jiang and H. Ji, "An empirical signal separation algorithm for multicomponent signals based on linear time-frequency analysis," *Mechanical Systems and Signal Processing*, vol. 121, no. 4, pp. 791–809, April 2019.

[13] M.D. van der Walt, "Empirical mode decomposition with shape-preserving spline interpolation," *Results in Applied Mathematics*, in press, 2020.

[14] L. Li and H. Ji, "Signal feature extraction based on improved EMD method," *Measurement*, vol. 42, pp. 796–803, June 2009.

[15] L. Cohen, *Time-frequency Analysis*, Prentice Hall, New Jersey, 1995.

[16] H. Hassanpour, M. Mesbah and B. Boashash, "SVD-based TF feature extraction for newborn EEG seizure," *EURASIP Journal on Advances in Signal Proc.*, vol. 16, pp. 2544–2554, 2004.

[17] L. Stanković, T. Thayaparan, and M. Daković, "Signal decomposition by using the S-method with application to the analysis of HF radar signals in sea-clutter," *IEEE Trans. Signal Proc.*, vol. 54, no. 11, pp. 4332–4342, Nov. 2006.

[18] L. Stanković, D. Mandić, M. Daković, and M. Brajović, "Time-frequency decomposition of multivariate multicomponent signals," *Signal Proc.*, vol. 142, pp. 468–479, Jan. 2018.

[19] I. Daubechies, J. Lu, and H.-T. Wu, "Synchrosqueezed wavelet transforms: An empirical mode decomposition-like tool," *Appl. Computat. Harmon. Anal.*, vol. 30, no. 2, pp. 243–261, Mar. 2011.

[20] I. Daubechies and S. Maes, "A nonlinear squeezing of the continuous wavelet transform based on auditory nerve models," in A. Aldroubi, M. Unser Eds. *Wavelets in Medicine and Biology*, CRC Press, 1996, pp. 527-546.

[21] F. Auger and P. Flandrin, "Improving the readability of time-frequency and time-scale representations by the reassignment method," *IEEE Trans. Signal Proc.*, vol. 43, no. 5, pp. 1068–1089, 1995.

[22] E. Chassande-Mottin, F. Auger, and P. Flandrin, "Time-frequency/time-scale reassignment," in *Wavelets and Signal Processing, Appl. Numer. Harmon. Anal.*, Birkhäuser Boston, Boston, MA, 2003, pp. 233–267.

[23] G. Thakur and H.-T. Wu, "Synchrosqueezing based recovery of instantaneous frequency from nonuniform samples," *SIAM J. Math. Anal.*, vol. 43, pp. 2078–2095, 2011.

[24] T. Oberlin, S. Meignen, and V. Perrier, "The Fourier-based synchrosqueezing transform," in *Proc. 39th Int. Conf. Acoust., Speech, Signal Process. (ICASSP)*, 2014, pp. 315–319.

[25] H.-T. Wu, *Adaptive Analysis of Complex Data Sets*, Ph.D. dissertation, Princeton Univ., Princeton, NJ, 2012.

[26] S. Meignen, T. Oberlin, and S. McLaughlin, "A new algorithm for multicomponent signals analysis based on synchrosqueezing: With an application to signal sampling and denoising," *IEEE Trans. Signal Proc.*, vol. 60, no. 11, pp. 5787–5798, Nov. 2012.

[27] F. Auger, P. Flandrin, Y. Lin, S.McLaughlin, S. Meignen, T. Oberlin, and H.-T. Wu, "Time-frequency reassignment and synchrosqueezing: An overview," *IEEE Signal Process. Mag.*, vol. 30, no. 6, pp. 32–41, 2013.

[28] C. Li and M. Liang, "Time frequency signal analysis for gearbox fault diagnosis using a generalized synchrosqueezing transform," *Mechanical Systems and Signal Proc.*, vol. 26, pp. 205–217, 2012.

[29] S.B. Wang, X.F. Chen, I.W. Selesnick, Y.J. Guo, C.W. Tong and X.W. Zhang, "Matching synchrosqueezing transform: A useful tool for characterizing signals with fast varying instantaneous frequency and application to machine fault diagnosis," *Mechanical Systems and Signal Proc.*, vol. 100, pp. 242–288, Feb. 2018.

[30] H.Z. Yang, J.F. Lu, and L.X. Ying, "Crystal image analysis using 2D synchrosqueezed transforms," *Multiscale Modeling & Simulation*, vol. 13, no. 4, pp. 1542–1572, 2015.

[31] J.F. Lu and H.Z. Yang, "Phase-space sketching for crystal image analysis based on synchrosqueezed transforms," *SIAM J. Imaging Sci.*, vol. 11, no. 3, pp.1954–1978, 2018.

[32] K. He, Q. Li, and Q. Yang, "Characteristic analysis of welding crack acoustic emission signals using synchrosqueezed wavelet transform," *J. Testing and Evaluation*, vol. 46, no. 6, pp. 2679–2691, 2018.

[33] H.-T. Wu, Y.-H. Chan, Y.-T. Lin, and Y.-H. Yeh, "Using synchrosqueezing transform to discover breathing dynamics from ECG signals," *Appl. Comput. Harmon. Anal.*, vol. 36, no. 2, pp. 354–459, Mar. 2014.

[34] H.-T. Wu, R. Talmon, and Y.L. Lo, "Assess sleep stage by modern signal processing techniques," *IEEE Trans. Biomedical Engineering*, vol. 62, no. 4, 1159–1168, 2015.

[35] C. L. Herry, M. Frasch, A. J. Seely1, and H. -T. Wu, "Heart beat classification from single-lead ECG using the synchrosqueezing transform," *Physiological Measurement*, vol. 38, no. 2, Jan. 2017.

[36] S. Wang, X. Chen, G. Cai, B. Chen, X. Li, and Z. He, "Matching demodulation transform and synchrosqueezing in time-frequency analysis," *IEEE Trans. Signal Proc.*, vol. 62, no. 1, pp. 69–84, 2014.

[37] Q.T. Jiang and B.W. Suter, "Instantaneous frequency estimation based on synchrosqueezing wavelet transform," *Signal Proc.*, vol. 138, no.9, pp.167–181, 2017.

[38] C. Li and M. Liang, "A generalized synchrosqueezing transform for enhancing signal time-frequency representation," *Signal Proc.*, vol. 92, no. 9, pp. 2264–2274, 2012.

[39] T. Oberlin, S. Meignen, and V. Perrier, "Second-order synchrosqueezing transform or invertible reassignment? towards ideal time-frequency representations," *IEEE Trans. Signal Proc.*, vol. 63, no. 5, p.1335–1344, Mar. 2015.

[40] T. Oberlin and S. Meignen, "The 2nd-order wavelet synchrosqueezing transform," in *2017 IEEE International Conference on Acoustics, Speech and Signal Processing (ICASSP)*, March 2017, New Orleans, LA, USA.

[41] D.H. Pham and S. Meignen, "High-order synchrosqueezing transform for multicomponent signals analysisWith an application to gravitational-wave signal," *IEEE Trans. Signal Proc.*, vol. 65, no. 12, p.3168–3178, Jun. 2017.

[42] L. Li, Z.H. Wang, H.Y. Cai, Q.T. Jiang, and H.B. Ji, "Time-varying parameter-based synchrosqueezing wavelet transform with the approximation of cubic phase functions," in *2018 14th IEEE Int'l Conference on Signal Proc. (ICSP)*, pp. 844–848, Aug. 2018.

[43] L. Li, H.Y. Cai, H.X. Han, Q.T. Jiang and H.B. Ji, "Adaptive short-time Fourier transform and synchrosqueezing transform for nonstationary signal separation," *Signal Proc.*, in press. arXiv:1812.11292

[44] L. Li, H.Y. Cai, and Q.T. Jiang, "Adaptive synchrosqueezing transform with a time-varying parameter for nonstationary signal separation," *Appl. Comput. Harmon. Anal.*, in press. arXiv:1812.11364.

[45] H.Y. Cai, Q.T. Jiang, L. Li, and B.W. Suter, "Analysis of adaptive short-time Fourier transform-based synchrosqueezing transform," preprint, 2018, arXiv:1812.11033.

[46] Y.-L. Sheu, L.-Y. Hsu, P.-T. Chou, and H.-T. Wu, "Entropy-based time-varying window width selection for nonlinear-type TF analysis," *Int'l J. Data Sci. Anal.*, vol. 3, pp. 231–245, 2017.

[47] A. Berrian and N. Saito, "Adaptive synchrosqueezing based on a quilted short-time Fourier transform," arXiv:1707.03138v5, Sep. 2017.

[48] C. K. Chui and H. N. Mhaskar, "Signal decomposition and analysis via extraction of frequencies," *Appl. Comput. Harmon. Anal.*, vol. 40, no. 1, pp. 97–136, 2016.

[49] V.C. Chen, F. Li, S.-S. Ho, and H. Wechsler, "Micro-Doppler effect in radar : phenomenon, model, and simulation study," *IEEE Trans. Aerosp. Electron. Syst.*, vol. 42, no. 1, pp. 2–21, 2006.

[50] L. Stanković, I. Orović, S. Stanković, and M. Amin, "Compressive sensing based separation of nonstationary and stationary signals overlapping in time-frequency," *IEEE Trans. Signal Proc.*, vol 61, no. 18, pp. 4562–4572, Sep. 2013.

[51] B. Barkat and K. Abed-Meraim, "Algorithms for blind components separation and extraction from the time-frequency distribution of their mixture," *EURASIP J. Appl. Signal Proc.*, vol. 13, pp. 2025–2033, 2004.

[52] S. Chen, X. Dong, G. Xing, Z. Peng, W. Zhang and G. Meng, "Separation of overlapped non-Stationary signals by ridge path regrouping and intrinsic chirp component decomposition,'' *IEEE Sensors Journals*, vol. 17, no. 18, pp. 5994–6005, Sep. 2017.

[53] V. Katkovnik, "A new form of the Fourier transform for time-frequency estimation,'' *Signal Proc.*, vol. 47, no. 2, pp. 187–200, 1995.

[54] X. Xia, "Discrete chirp-Fourier transform and its application to chirp rate estimation," *IEEE Trans. Signal Proc.*, vol. 48, no. 11, pp. 3122-3133, Nov. 2000.

[55] X. Li, G. Bi, S. Stankovic and A.M. Zoubir, "Local polynomial Fourier transform: A review on recent developments and applications," *Signal Proc.*, vol. 91, no.6, pp.1370–1393, 2011.

[56] S. Mann and S. Haykin, "The chirplet transform: Physical considerations," *IEEE Trans. Signal Proc.*, vol. 43, no. 11, pp. 2745–2761, Nov. 1995.

[57] R. G. Baraniuk and D. L. Jones, "Wigner-based formulation of the chirplet transform," *IEEE Trans. Signal Proc.*, vol. 44, no. 12, pp. 3129–3135, Dec. 1996.

[58] J. Zheng J, H. Liu and Q. Liu, "Parameterized centroid frequency-chirp rate distribution for LFM signal analysis and mechanisms of constant delay introduction," *IEEE Trans. Signal Proc.*, vol. 65, no. 24, pp. 6435–6447, Dec. 2017.

[59] K. Czarnecki, D. Fourer, F. Auger and M. Rojewski, "A fast time-frequency multi-window analysis using a tuning directional kernel," *Signal Processing*, vol. 147, pp. 110–119, Jun. 2018.

[60] L. Stanković, M. Daković, and T. Thayaparan, *Time-Frequency Signal Analysis with Applications*, Artech House, Boston, 2013.

[61] G. Beylkin, "Discrete radon transform," *IEEE Trans. Acoust. Speech Signal Process.*, vol. 35, no. 2, pp. 162-172, Feb. 1987.

[62] A. Averbuch and Y. Shkolnisky, "3D Fourier based discrete Radon transform," *Appl. Comput. Harmon. Anal.*, vol. 15, pp. 33–69, July 2003.

[63] M. Wang, A.K. Chan and C.K. Chui, "Linear frequency-modulated signal detection using Radon-ambiguity transform," *IEEE Trans. Signal Proc.*, vol. 46, no. 3, pp. 571-586, Mar. 1998.